Characterization of Eocene lacustrine source rocks and their oils in the Beibuwan Basin, offshore South China Sea

Baojia Huang, Weilin Zhu, Hui Tian, Qiuyue Jin, Xianming Xiao, and Chenhui Hu

ABSTRACT

A total of 225 rock samples and 37 oil samples from the Beibuwan Basin, South China Sea, were analyzed with geochemical and organic petrological techniques to evaluate the Eocene lacustrine source rocks and investigate controls on their properties and the distribution of different oil families in the basin. Two types of organic facies are recognized in the Liushagang Formation (LS). The first organic facies is algal-dominated and mainly occurs in the organic-rich, laminated mudstones of the middle member of the LS (LS-2) that were deposited in an anoxic, stratified, medium–deep lake environment. It is geochemically identified by its high abundance of C_{30} 4-methylsteranes and heavy $\delta^{13}C$ values in the range of –22.4‰ to –27.5‰. The organic matter in this organic facies comprises type I and II_1 kerogens, with its macerals dominated by fluorescent amorphous organic matter (AOM) and exinites, indicating a highly oil-prone character. The second organic facies is of terrestrial algal origin and is mainly identified in the nonlaminated mudstones of the upper (LS-1) and lower (LS-3) members of the LS that were deposited in shallow, dysoxic, weakly stratified, freshwater environments. Source rocks of the second organic facies mainly contain type II_1–II_2 kerogens with mixed macerals of AOM, internites, and vitrinites. It is geochemically differentiated from the algal-dominated organic facies by its relatively low abundance of C_{30} 4-methylsteranes and lighter $\delta^{13}C$ values in the range of –27.20‰ to –28.67‰. Three oil groups are identified by their biomarkers and stable carbon isotopes. The first two groups (A and B) are probably end-members of two major oil families (A and B) that correspond to the algal-dominated organic facies and algal–terrestrial organic facies, respectively. Most of the discovered oils belong

Manuscript received August 19, 2015; provisional acceptance April 14, 2016; revised manuscript received August 15, 2016; final acceptance October 17, 2016.
DOI:10.1306/10171615161

AUTHORS

BAOJIA HUANG ~ *State Key Laboratory of Organic Geochemistry, Guangzhou Institute of Geochemistry, Chinese Academy of Sciences, 511 Kehua Street, Tianhe District, Guangzhou 510640, China; present address: Research Institute, Zhanjiang Branch, China National Offshore Oil Corporation Ltd, Post Box 22, Potou District, Zhanjiang 524057, China; huangbj@cnooc.com.cn*

Baojia Huang is a guest professor at the Guangzhou Institute of Geochemistry, Chinese Academy of Sciences, where he received his Ph.D. in geochemistry in 2002, and a senior geologist at the Research Institute, Zhanjiang Branch of China National Offshore Oil Corporation Ltd. His main research interests include petroleum geochemistry and petroleum systems, with particular attention to the generation and accumulation of hydrocarbons.

WEILIN ZHU ~ *China National Offshore Oil Corporation Ltd, 25 North Chaoyangmen, Dongcheng District, Beijing 100010, China; zhuwl@cnooc.com.cn*

Weilin Zhu is chief geologist at China National Offshore Oil Corporation. He received his Ph.D. in 2001. His main research interests include petroleum systems, basin analysis, and risk evaluation of petroleum exploration.

HUI TIAN ~ *State Key Laboratory of Organic Geochemistry, Guangzhou Institute of Geochemistry, Chinese Academy of Sciences, 511 Kehua Street, Tianhe District,Guangzhou 510640, China; tianhui@gig.ac.cn*

Hui Tian is a professor at the Guangzhou Institute of Geochemistry, Chinese Academy of Sciences, where he received his Ph.D. in geochemistry in 2006. He received his B.S. and M.S. degrees in petroleum geology from the University of Petroleum, China, in 2000 and 2003, respectively. His recent and current research focuses on the formation and preservation of oil and gas in sedimentary basins. He is the corresponding author of this article.

QIUYUE JIN ~ *Research Institute, Zhanjiang Branch, China National Offshore Oil*

Corporation Ltd, Post Box 22, Potou District, Zhanjiang 524057, China; jinqy@cnooc.com.cn

Qiuyue Jin is a geologist at the Research Institute, Zhanjiang Branch of China National Offshore Oil Corporation Ltd. His research interests are petroleum geochemistry and petroleum systems, with particular attention to the petroleum biomarkers and stable isotopes.

XIANMING XIAO ~ *State Key Laboratory of Organic Geochemistry, Guangzhou Institute of Geochemistry, Chinese Academy of Sciences, 511 Kehua Street, Tianhe District, Guangzhou 510640, China; xmxiao@gig.ac.cn*

Xianming Xiao is a professor at the Guangzhou Institute of Geochemistry, Chinese Academy of Sciences. He received his Ph.D. in geology from the Beijing University of Mining and Technology in 1989. His current research interests include the dynamics of petroleum accumulation, with particular attention to hydrocarbon generation kinetics and paleopressure reconstruction using fluid inclusion information.

CHENHUI HU ~ *Research Institute, Zhanjiang Branch, China National Offshore Oil Corporation Ltd, Post Box 22, Potou District, Zhanjiang 524057, China; huchh1@cnooc.com.cn*

Chenhui Hu is a geologist at the Research Institute, Zhanjiang Branch of China National Offshore Oil Corporation Ltd. His main research interest is petroleum geochemistry, with particular attention to the petroleum biomarkers and petroleum migration.

ACKNOWLEDGMENTS

We are extremely grateful to Shu Jiang of the University of Utah, who helped polish the English language. Harry Doust, Jessica E. Little, Barry J. Katz, and one anonymous AAPG reviewer are acknowledged for their constructive comments and suggestions that significantly improved the manuscript. Special thanks go to Barry Katz and AAPG staff for their editorial work that makes the geological terms used in this manuscript as accurate as possible. The authors are indebted to Zhanjiang Branch of China National Offshore Oil Corporation Ltd for

to group A oils that are characterized by a high abundance of C_{30} 4-methylsteranes and heavy $\delta^{13}C$ values and show a good correlation with the algal-dominated organic facies in LS-2. Group B oils are found only within the LS-1 and LS-3 reservoirs, and they are recognized by their relatively low content of C_{30} 4-methylsteranes and lighter $\delta^{13}C$ values, showing a close relation to the algal–terrestrial source facies within the LS-1 and LS-3 members, respectively. Group C oils display intermediate biomarker features and stable carbon isotope values and are interpreted to be a mixture of group A and B oils. The oil–source correlation reveals a strong control of organic facies on the geographic distribution of oil groups or oil fields in the basin.

INTRODUCTION

Lacustrine shales have been recognized as important source rocks in many continental rift basins, e.g., Cretaceous basins of central, western, and eastern Africa; Paleozoic basins of western China; and Paleogene–Neogene basins of eastern China and southeastern Asia (Katz, 1995a, b; Harris et al., 2004; Ji et al., 2011; Rodriguez and Philp, 2015). Greater than 20% of the hydrocarbon production worldwide is probably related to lake-associated deposits (Bohacs et al., 2000). The Beibuwan (BBW) and Pearl River Mouth Basins in the South China Sea are examples of petroliferous lacustrine basins, where the dominant source rocks are Paleogene lacustrine mudstones (Robison et al., 1998; Huang et al., 2003, 2013; Zhu and Wu, 2004). The BBW Basin is located in the northern continental margin of the South China Sea and covers an area of nearly 40,000 km^2 (15,440 mi^2) (Figure 1A). Over the past 30 yr, exploration in this basin has been focused on the Weixinan and Wushi subbasins, where some oil fields and numerous oil-bearing structures have been discovered (Figure 1B), with estimated oil resources greater than 350 million tons (approximately 2500 million bbl) (Wang et al., 2014). These oils are discovered in Miocene, Oligocene, and Eocene sandstones and the Carboniferous burial hill carbonate basement at depths ranging from 1000 to 3500 m (3281 to 11,483 ft).

Both the stratigraphic distribution of potential source rocks and occurrences of oil reservoirs at different burial depths imply complex scenarios of petroleum generation, migration, and accumulation throughout the basin history. Previous studies focused on the Weixinan subbasin and revealed that the Eocene Liushagang Formation probably sourced all of the discovered oils (Zhu and Wu, 2004; Huang et al., 2013); however, the distribution of high-quality source rocks and the origin of some oils reservoired in the Oligocene Weizhou Formation away from the Eocene source rocks remain uncertain. Moreover, very little work has been published on the basin's southern flank, which extends into the

Wushi subbasin. In this study, an extensive sampling and analytical program was undertaken in the Wushi and Weixinan subbasins to describe the organic facies in much greater detail than previously known and identify key oil families or groups and their corresponding organic facies or stratigraphic units that sourced them through distinctive molecular and stable carbon isotopic features. These results will help better understand the petroleum system in the basin and identify the exploration risk in this area.

GEOLOGICAL SETTINGS

The BBW Basin is one of the four petroliferous basins on the northern continental shelf of the South China Sea (Gong and Li, 1997; Zhu and Mi, 2010). It is a Mesozoic–Cenozoic extensional basin, containing three uplifts and seven Paleogene subbasins that formed in response to tectonic extension during the late Paleocene (Figure 1A). The Paleogene–Neogene tectonic evolution can be divided into an Eocene to Oligocene extensional phase marked by the formation of fault-bounded, rifted subbasins and a Miocene to Holocene passive margin phase characterized by relatively unstructured strata, leading to two distinctive tectonic sequences (Figure 2). The tectonic extension of the basin is believed to be related to both the southward slab pulling by the subduction of oceanic crust of the proto–South China Sea and the extrusion and clockwise rotation of Indochina along the Red River Fault (Ru and Pigott, 1986; Gong and Li, 1997).

In response to the structural evolution, the depositional environments in the BBW Basin evolved from continental nonmarine fluvial and lacustrine facies during the Paleocene–Oligocene to transgressive marine facies during the Miocene (Figure 2), forming synrift and postrift rocks, respectively. Incipient rifting during the Paleocene resulted in the deposition of the Changliu Formation, which is predominantly composed of coarse-grained, matrix-supported conglomerate, overlies directly the Mesozoic–Paleozoic basement unconformity, and is adjacent to highly active fault scarps (Zhu and Wu, 2004; Zhu and Mi, 2010).

The Eocene–Oligocene rifting includes two significant synrift phases represented by the Liushagang Formation (LS) and the Weizhou Formation, respectively (Figure 2). The Eocene LS is approximately 1000–2500 m (3281–8202 ft) thick in the Weixinan and Wushi subbasins and mainly consists of black shales, siltstones, and sandstones. The lacustrine shales can be easily recognized in seismic sections, showing synrift successions with distinct, continuous high-amplitude reflections. Based on lithology and fossil assemblages, the LS is subdivided into upper, middle, and lower members: Liushagang-1 (LS-1), Liushagang-2 (LS-2), and Liushagang-3 (LS-3), respectively (Li, 1994). The LS-3 member

making the oil and rock samples available. This work was financially supported by National Science and Technology Major Project of China (Grant 2016ZX05024002-009), the National Natural Science Fund of China (41522302), Guangzhou Institute of Geochemistry, Chinese Academy of Sicences (No. IS-2314), and the Tuguangchi Talent Foundation (GIGRC-10-02). This is contribution No.IS-2314 from GIGCAS.

EDITOR'S NOTE

Color versions of Figures 1, 3–11, and 13–19 can be seen in the online version of this paper.

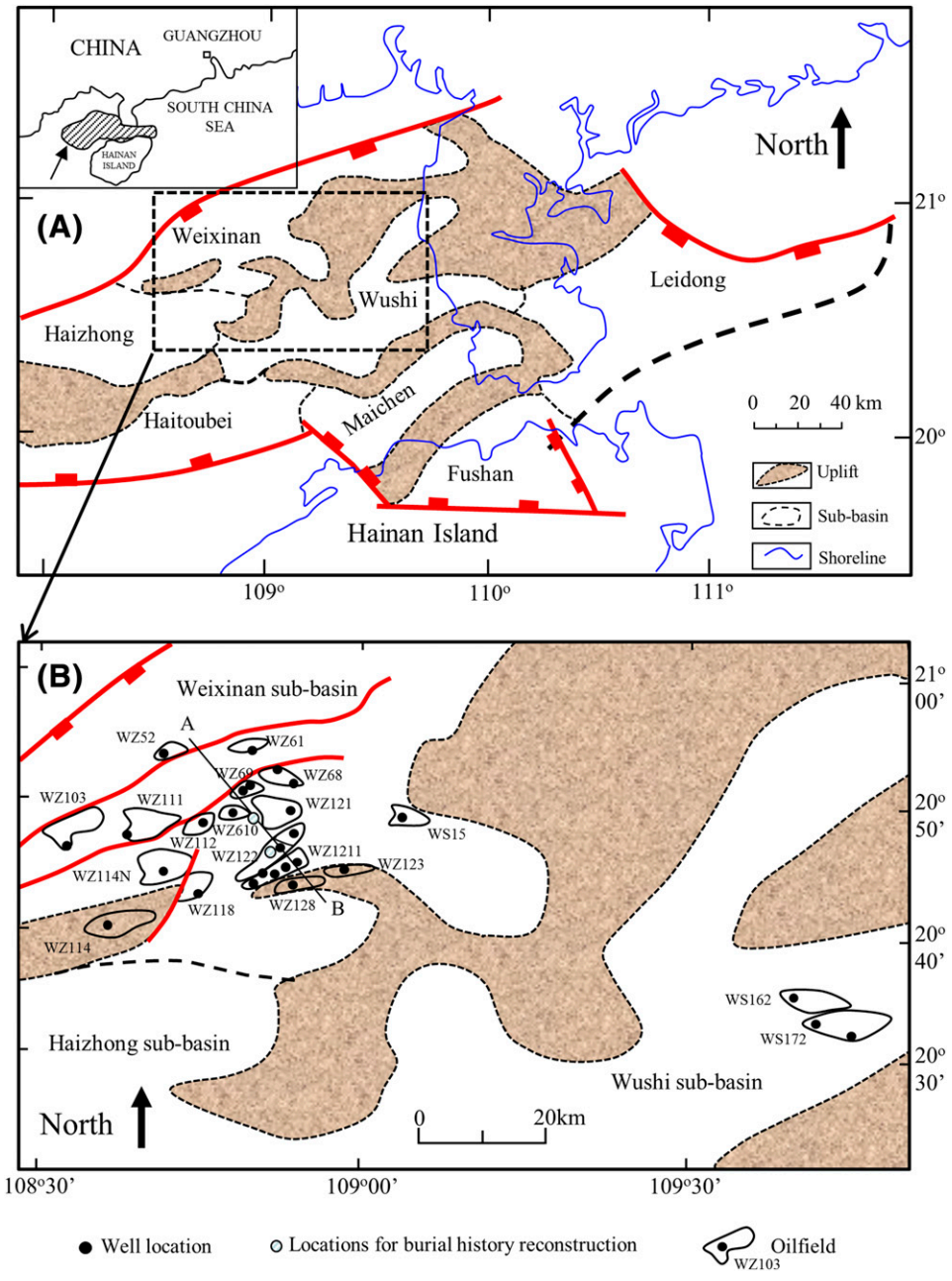

Figure 1. Maps showing (A) structural divisions of the Beibuwan Basin and (B) sampling wells in the Weixinan and Wushi sub-basins. LS-1 = upper member of the Liushagang Formation; LS-2 = middle member of the Liushagang Formation; LS-3 = lower member of the Liushagang Formation; WZ = Weizhou Formation.

contains approximately 200 m (656 ft) of interbedded sandstones and shales that were deposited in shallow lake and fluvial facies with low to moderate energies (Sun et al., 2008; Song et al., 2012). In response to a subsequent lake transgression, the organic-rich LS-2 was formed under anoxic environments in a medium–deep lake (Figure 2), with a gross thickness of up to 300–500 m (984–1640 ft); where lacustrine deltaic progradation was active, a thick sequence was locally formed of interbedded fine-grained sandstones and shales (Liu, 2004; Sun et al., 2008). During the late Eocene, a shallow lake facies prevailed and formed a set of interbedded sandstones and shales that composes LS-1 (Sun et al., 2008; Song et al., 2012). The Weizhou Formation comprises thick sandstones formed under moderate- to high-energy fluvial environments with interbedded shales and silty shales deposited in a flood plain or shallow lake setting, thus forming an important reservoir–seal assemblage (Wang et al., 2014).

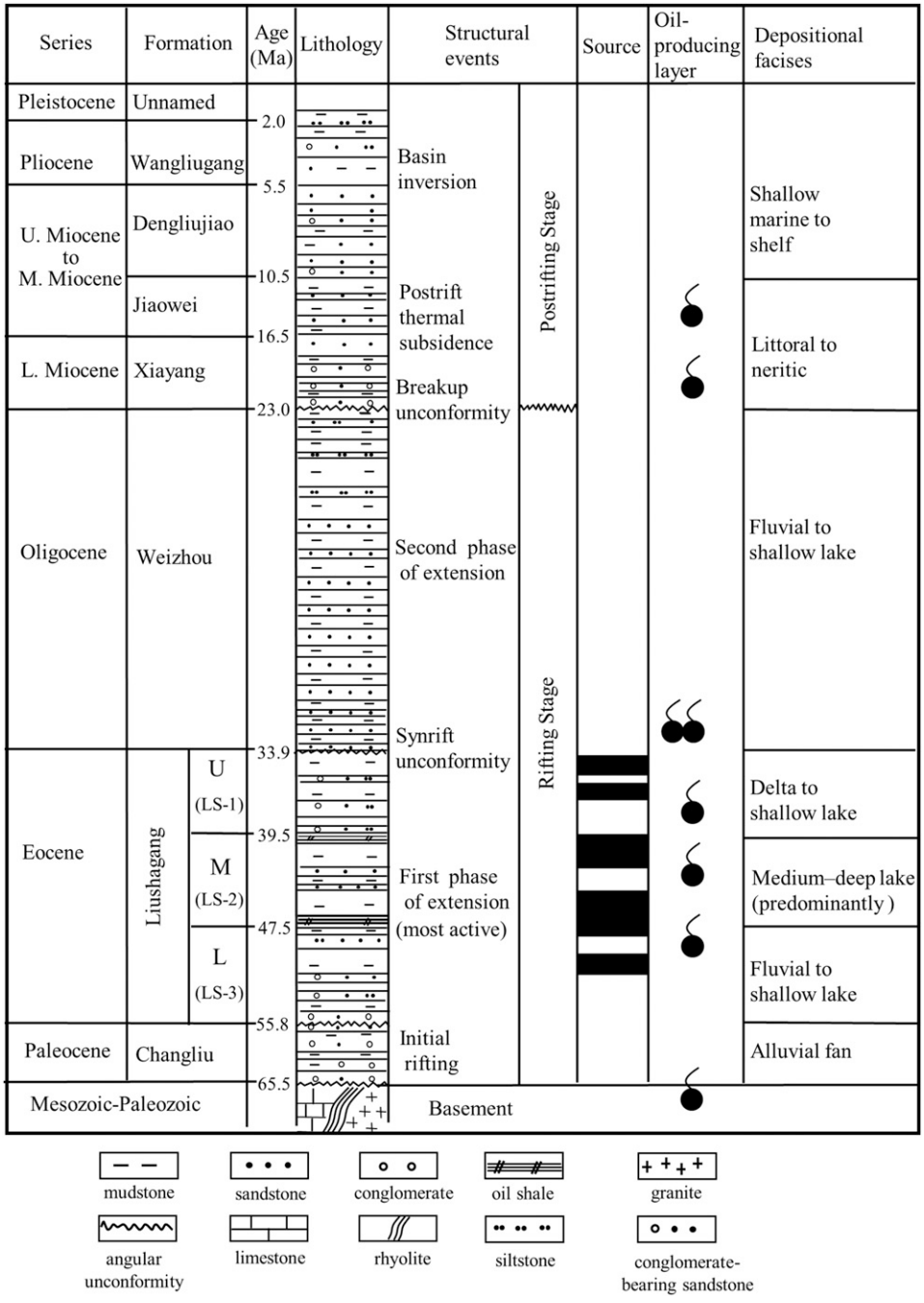

Figure 2. Schematic stratigraphy of the Beibuwan Basin. L. = lower; LS-1 = upper member of the Liushagang Formation; LS-2 = middle member of the Liushagang Formation; LS-3 = lower member of the Liushagang Formation; M. = middle; U. = upper.

The top of the Weizhou Formation is marked by a significant regional unconformity surface, which defines the boundary between the synrift and postrift (passive) sedimentary fillings of the BBW Basin (Sun et al., 2008). The postrift marine rocks of the Miocene–Pleistocene consist mainly of sandstones interbedded with mudstones and have a total thickness of approximately 3000 m (9842 ft) (Figure 2) and are considered excellent regional seals for hydrocarbons (Zhu and Mi, 2010; Song et al., 2012).

SAMPLES AND EXPERIMENTS

A total of 225 cutting and core samples were obtained from 10 wells, and a total of 37 oil samples were collected from 25 oil-producing wells during drill stem tests or module formation tests in the Weixinan and Wushi subbasins. Locations of sampling sites are shown in Figure 1B. Total organic carbon (TOC) was determined with a LECO CS 200 carbon–sulfur analyzer by combusting the rock samples that were

pretreated with dilute hydrochloric acid; Rock-Eval analysis was carried out on original samples using a Rock-Eval6 instrument with a standard program (Espitalié, et al., 1977; Lafargue et al., 1998).

Selected source rock samples with TOC values greater than 2 wt. %, except for one sample from the LS-3 member with a TOC value of 0.8 wt. %, were ground and Soxhlet extracted with dichloromethane (DCM, 72 h). The asphaltenes were removed from the DCM extracts and oils by adding at least 40-fold excess hexane. Then, the deasphalted DCM extracts and oils were fractioned using column chromatography, and saturate fractions were analyzed using a Hewlett–Packard 6890II gas chromatograph equipped with a 50 m × 0.32 mm i.d. (164 ft × 0.01 in.) HP-5 fused silica capillary column. The carrier gas was helium at a flow rate of 1.5 mL/min (0.05 fl oz/min). The samples were injected using a splitless injector maintained at 300°C (572°F). The gas chromatography (GC) oven temperature was programmed from 35°C to 300°C (95°F to 572°F) at 5°C/min (40°F/min) and maintained at the final temperature for 30 min. Gas chromatography–mass spectrometric analyses (GC-MS) were carried out using a Thermo Fisher Scientific Trace GC Ultra gas chromatograph connected to a DSQ II mass spectrometer. Helium was used as carrier gas, and the oven temperature was programmed from 50°C to 300°C (122°F to 572°F) at 4°C/min (39°F/min). Samples were routinely analyzed in a full scan mode (mass-to-charge ratio [*m/z*] 50–500). Compound identification and quantification were based on known standards and published documents. The identifications on C_{30} 4-methylsteranes were based on a combination of mass chromatograms (*m/z* 217, 231, and 414), individual mass spectra, and GC retention times. The stable carbon isotopes ($\delta^{13}C$) of oils and kerogens were determined using a Finnigan MAT-251 mass spectrometer. The $\delta^{13}C$ values are reported relative to the Peedee belemnite standard, with an analytical precision of ±0.3‰.

Approximately 20 rock samples were prepared for organic petrological analysis using a standard coal petrographic method (Tyson, 1993). The one-side polished blocks were petrographically examined in transmitted light and fluorescence modes. Quantitative analyses of palynomorph variation were made on 60 kerogen samples, which were prepared following the normal treatment of cores and cuttings with

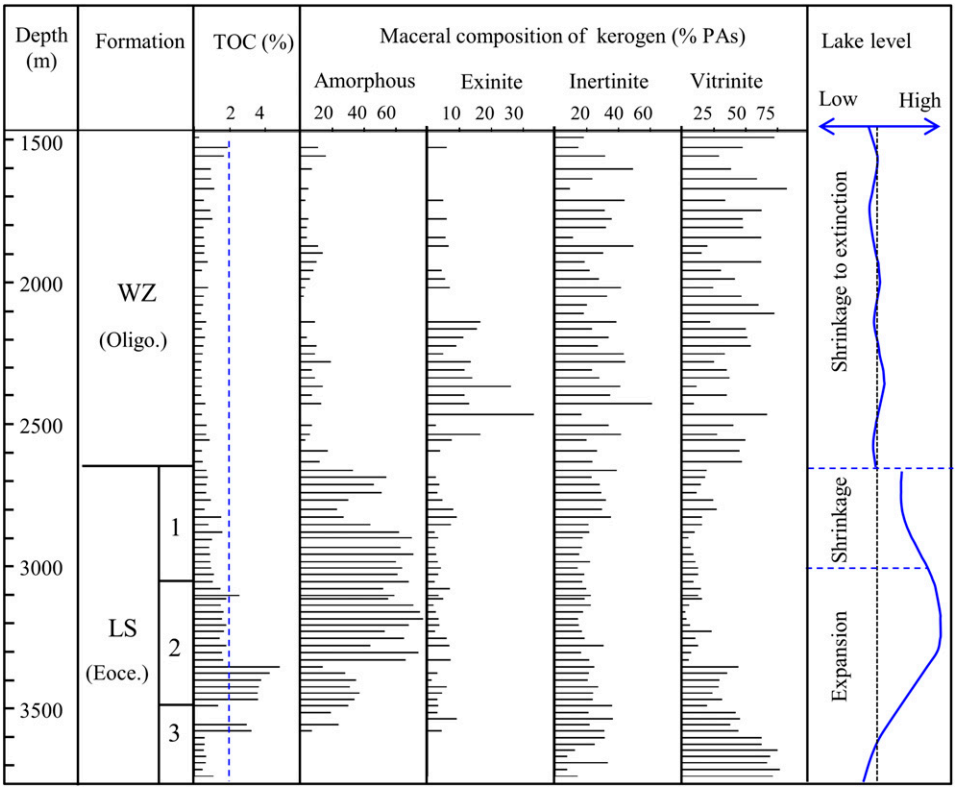

Figure 3. Maceral composition profile of kerogens isolated from the Eocene Liushagang Formation (LS) source rocks for the WZ112 well (see Figure 1 for well location). The shales in middle member of the Liushagang Formation (LS-2) and lower part of upper member of the Liushagang Formation (LS-1) are characterized by abundant amorphous organic matter. % PAs = relative percentage of particle abundance; Eoce. = Eocene; LS-3 = lower member of the Liushagang Formation; Oligo. = Oligocene; TOC = total organic carbon; WZ = Weizhou.

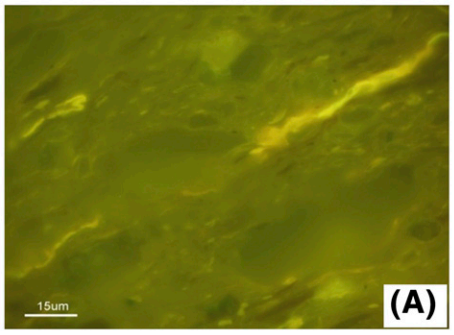

WS172 well, shale, 2370–2374m (7776–7789ft)
Orange-yellowish fluorescing lamalginites

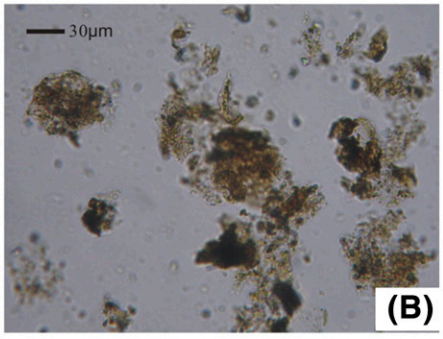

WZ112 well, kerogen, 2892m (9489ft)
Abundant amorphous organic matter

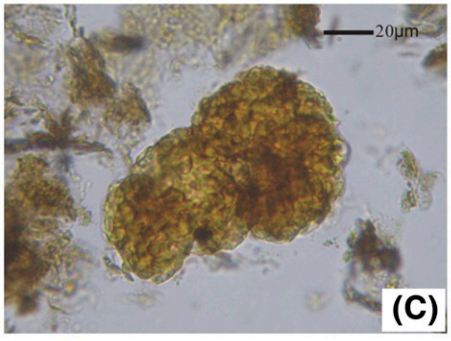

WS172 well, kerogen, 2280m (7481ft)
Botryococcus

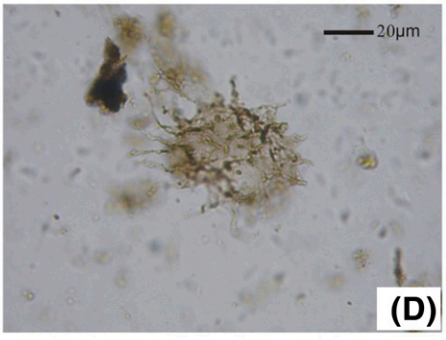

WZ112 well, kerogen, 3176m (10,420ft)
Pediastrum

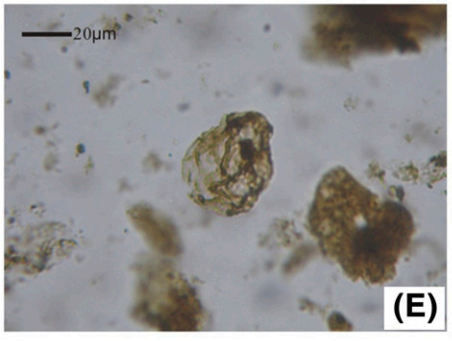

WZ112 well, kerogen, 3152m (10,342ft)
Pediastrum

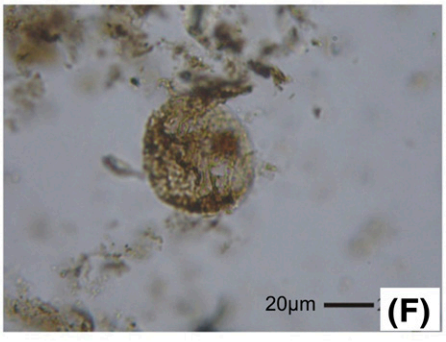

WZ112 well, kerogen, 3128m (10,263ft)
Granodiscus

Figure 4. Photomicrographs of macerals in the shales and their kerogens of Liushagang Formation under (A) blue-light excited fluorescence mode and (B–F) transmitted white light. WS = Wushi; WZ = Weizhou.

hydrochloric acid, hydrofluoric acid, and zinc bromide (Tyson, 1993). One slide per sample was analyzed under the microscope, and kerogen counts were performed by making a series of three or more traverses across the slide until a total of 500 maceral particles were counted for each sample. The data generated by the kerogen counting procedure are expressed as relative percentage of particle abundances. Photomicrographs were taken using a QImaging MicroPublisher 5.0 RTV camera attached directly to a personal computer and converted to digital images.

RESULTS AND DISCUSSION

Organic Facies

Two organic facies can be recognized in the Liushagang Formation by combining palynological, organic petrological data with biomarkers and stable carbon isotopes (Figures 3–9).

The first organic facies consists of black shales formed in a medium–deep lake setting and mainly comprises samples from the LS-2 source rocks. The organic matter in these source rocks is dominated by

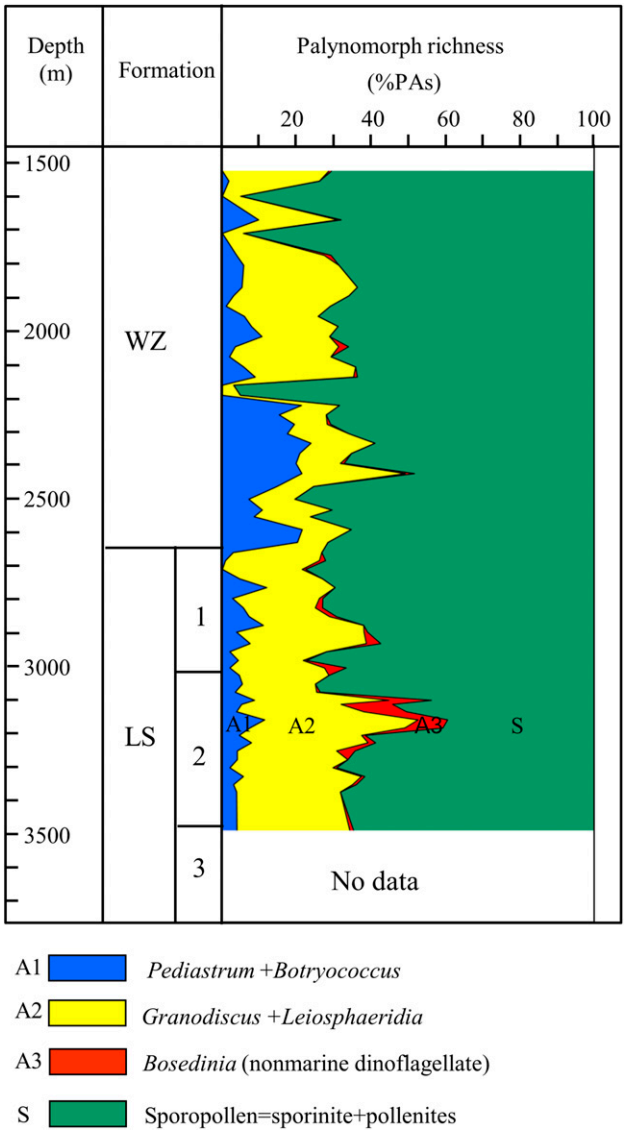

Figure 5. Palynomorph richness of the Liushagang Formation (LS) for the WZ112 well (see Figure 1 for well location). The organic-rich shales are characterized by abundant alginite. %PAs= relative percentage of individual particle abundance; WZ = Weizhou Formation.

fluorescing amorphous organic matter (AOM) and exinite (Figures 3, 4A, B); the organic-rich LS-2 shale samples contain numerous lamalginites (Figure 4A). This organic facies is also called an algal-dominated organic facies. The common association of alginite with fluorescing AOM and liptodetrinite suggests that latter two components both were derived, to a large extent, from the degradation of algal material. Some LS-2 samples contain a very high proportion of *Granodiscus* and *Leiosphaeridia* alginites (Figures 4F, 5), further supporting the above interpretation. Microscopic examination indicates that the kerogens contain 70%–80% AOM with 10%–15% exinite and 10%–30% vitrinite and inertinite (Figure 3), and thus, they are classified mainly as oil-prone kerogens of types I and II_1 with minor type II_2 kerogen according to the Rock-Eval data (Figure 6).

The other organic facies is mainly identified within the LS-1 and LS-3 members and the marginal lacustrine facies of the LS-2 member, where the source rocks were formed within shallow lake depositional environments. Compared with the first organic facies, this organic facies contains a greater proportion of terrigenous organic matter. As shown in Figure 3, the organic maceral composition in the LS-3 and the upper part of the LS-1 samples displays a smaller proportion of AOM (30%–40%) than in the LS-2 samples, whereas more terrigenous organic components (i.e., inertinite and vitrinite) are observed in the LS-1 and LS-3 samples than in the LS-2 samples. This organic facies can be defined as

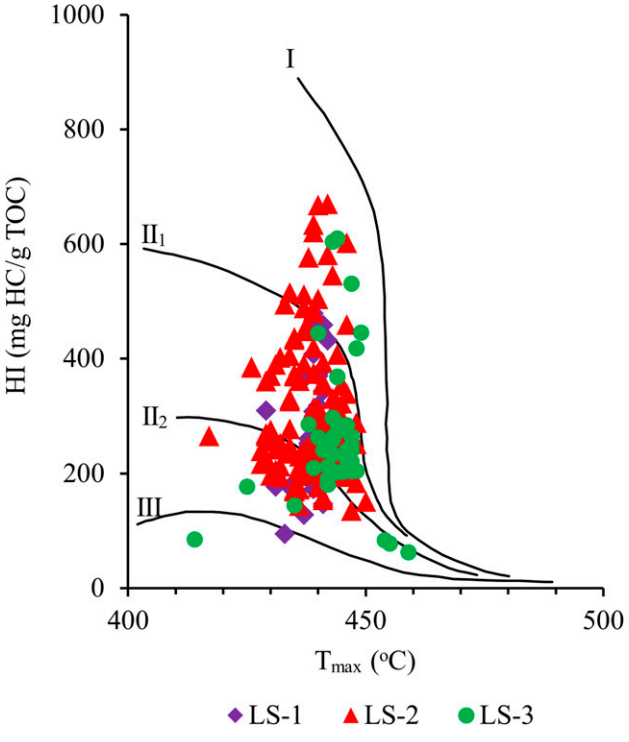

Figure 6. A plot of hydrogen index (HI) vs. pyrolysis temperature of maximum rate of hydrocarbon generation (T_{max}) showing the kerogen types of possible source rocks in the Liushagang Formation. HC = hyrdocarbons; LS-1 = upper member of the Liushagang Formation; LS-2 = middle member of the Liushagang Formation; LS-3 = lower member of the Liushagang Formation; TOC = total organic carbon.

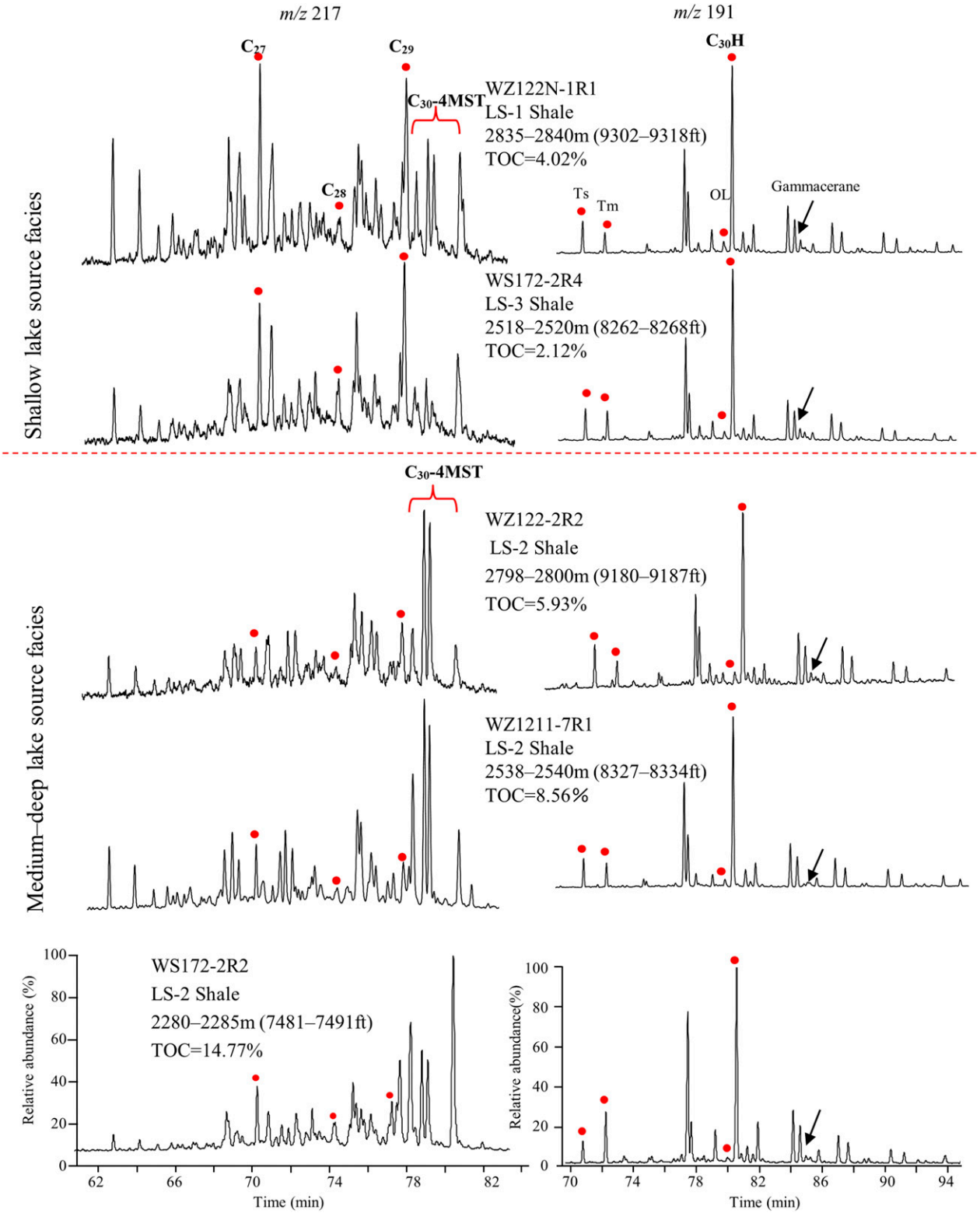

Figure 7. Mass-to-charge ratio (*m/z*) 191 and 217 mass chromatograms of extracts from the selected source rocks of Liushangang Formation in the Beibuwan Basin. C_{27}, C_{28}, and C_{29} = C_{27}, C_{28}, and $C_{29}\alpha\alpha\alpha$ 20R steranes; C_{30}-4MST = C_{30} 4-methylsteranes; C_{30}H = C_{30} $\alpha\beta$ hopane; LS-1 = upper member of the Liushagang Formation; LS-2 = middle member of the Liushagang Formation; LS-3 = lower member of the Liushagang Formation; MST = methylsteranes; OL = oleanane; Tm = 17α-trisnorhopane; Ts = 18α-trisnorhopane; TOC = total organic carbon; WS = Wushi; WZ = Weizhou.

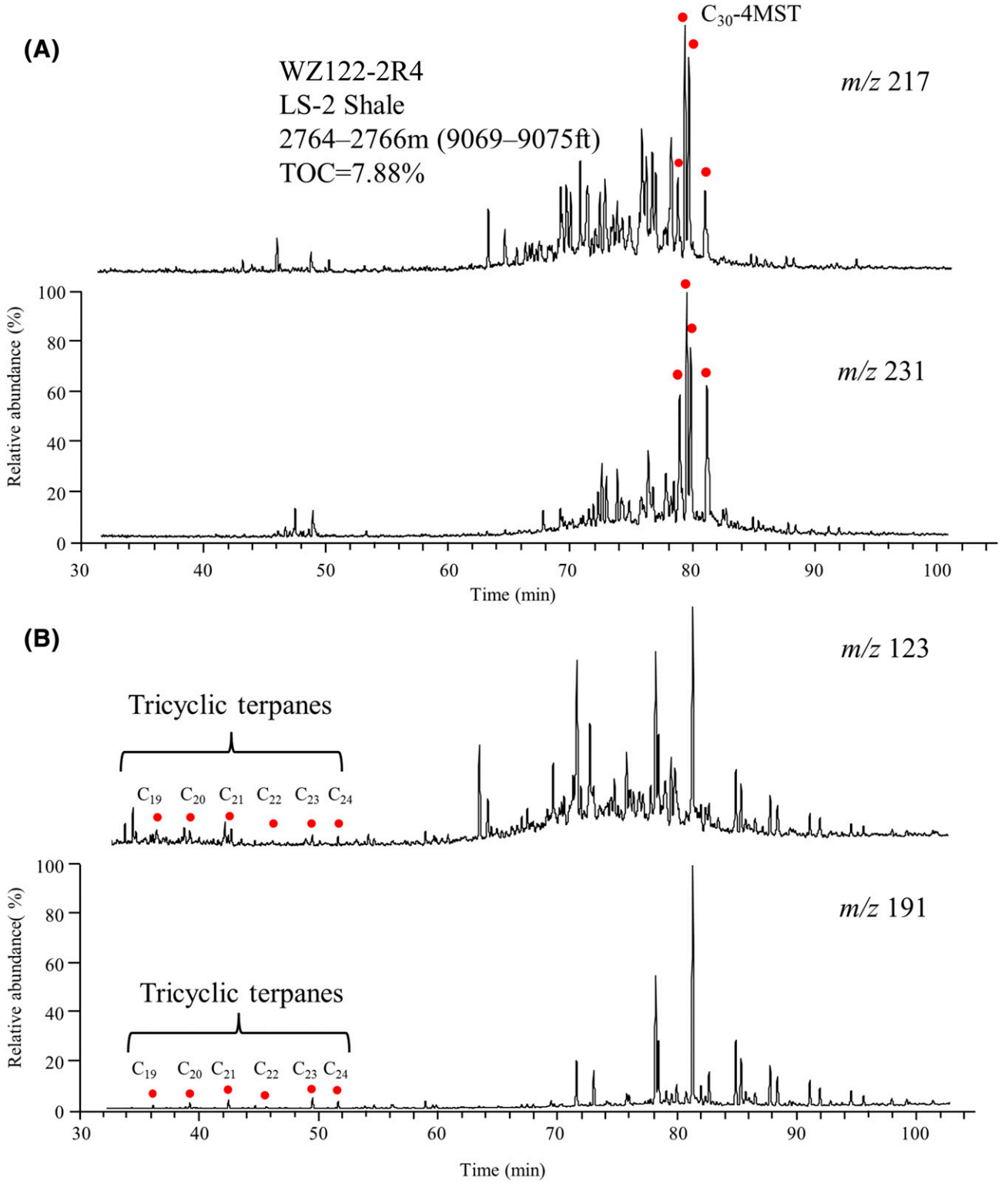

Figure 8. Selected mass chromatograms of the saturated hydrocarbon fractions from the middle member of the Liushagang Formation (LS-2) shales deposited in medium–deep lake facies. (A) Mass-to-charge ratio (*m/z*) 217 and *m/z* 231 chromatograms showing the distribution patterns of regular steranes and C_{30} 4-methylsteranes and (B) *m/z* 191 and *m/z* 123 chromatograms showing the very low or traces of diterpanes. C_{30}-4MST = C_{30} 4-methylsteranes; TOC = total organic carbon; WZ = Weizhou.

an algal–terrigenous organic facies. Microscopic observation reveals that their kerogens compromise 20%–30% exinite, 20%–70% vitrinite and inertinite, and 5%–50% AOM (Figure 3), indicating type II_1–II_2 kerogens with minor type I and III kerogens (Figure 6).

Distinct differences in biomarkers are also observed between the two organic facies. As shown in Figures 7 and 8A, the biomarkers for the shales from the medium–deep lake facies are characterized by an obvious predominance of C_{30} 4-methylsteranes over C_{29} regular steranes. Ratios of C_{30} 4-methylsteranes to C_{29} regular steranes (C_{30}-4MSI) range from 1.48 to 7.64 (Table 1). The C_{30} 4-methylsteranes are common biomarkers of the Cenozoic lacustrine rocks in eastern and northwestern China basins (Huang et al., 2003, 2013; Ji et al., 2011). Their biological precursors are probably related to certain dinoflagellates thriving in freshwater lakes (Brassell et al., 1988; Goodwin et al., 1988; Peters et al., 2005; Ji et al., 2011). The Eocene oil shales in the adjacent onshore Maoming Basin reveal that dinoflagellates are mainly enriched in high-quality hydrocarbon source rocks (with abundant C_{30} 4-methylsteranes) that are largely deposited in medium–deep, freshwater lake facies (Brassell et al., 1988). Dinoflagellates are not only the main source of sedimentary C_{30} 4-methylsteranes but also good parent materials for hydrocarbons in the Mesozoic and Cenozoic basins (Goodwin et al., 1988; Thomas et al., 1993). Thus, abundant C_{30} 4-methylsteranes detected in the LS-2 shale samples imply that dinoflagellates flourished in the lake during its deposition period.

At the same time, the oleanane, which is derived from angiosperm plants (Rullkötter et al., 1994), is in very low concentrations in the LS-2 samples, and the oleanane/C_{30}H ratios are in the range of 0.02–0.08. Murray et al. (1997) illustrated that the contact of land plant organic matter with seawater during early diagenesis would enhance the expression of oleanane in a mature sediment or oil. For our present samples of the Liushagang Formation, they were deposited, however, in freshwater lake and are not expected to be significantly affected by following seawater intrusion (Zhu, 2009; Huang et al., 2013). Therefore, the oleanane in the present samples is believed to provide valuable source information. In addition, tricyclic diterpanes, which are molecular indicators of

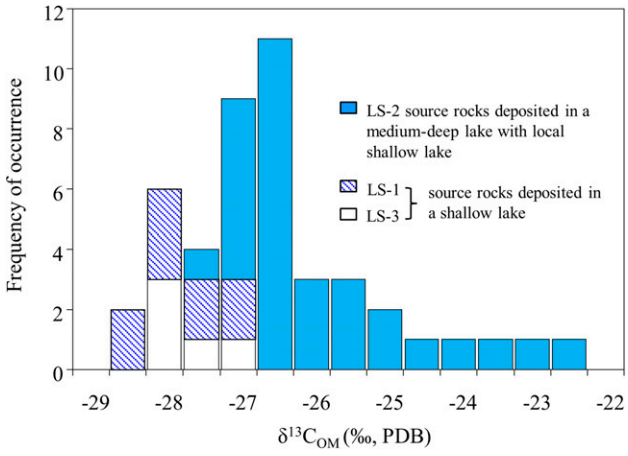

Figure 9. Stable carbon isotopes of kerogens ($\delta^{13}C_{OM}$) from different organic facies of the Eocene Liushagang Formation in the Beibuwan Basin, showing distinct carbon isotopic compositions between the two organic facies. LS-1 = upper member of the Liushagang Formation; LS-2 = middle member of the Liushagang Formation; LS-3 = lower member of the Liushagang Formation; OM = organic matter; PDB = Peedee belemnite.

terrigenous plant-derived organic matter (Alexander et al., 1987), were also detected in very low concentrations, and no isopimaranes were observed in the extracts of LS-2 shales (Figure 8B). Those results are consistent with the low oleanane contents and indicate a low input of terrigenous organic matter to the LS-2 medium–deep lake shales. In contrast, the source rocks from shallow lake organic facies are characterized by their low–moderate abundance of C_{30} 4-methylsteranes with a C_{30}-4MSI of 0.93–1.68 (Figure 7, Table 1), though they also have low oleanane/C_{30}H ratios (0.06–0.12), except for a few high values for samples from the LS-3 member.

Evident difference is also observed between the two distinct organic facies in the stable carbon isotopes of isolated kerogens. The stable carbon isotopes of kerogens isolated from shales from the medium–deep lake facies show $\delta^{13}C$ values in the range of –22.4‰ to –27.5‰, approximately 3‰–5‰ heavier than those of the kerogens from shallow lake facies (Figure 9). These data seem inconsistent with the general isotopic compositions of kerogens from the Mesozoic–Cenozoic sedimentary basins in eastern China, where type III kerogens are commonly more enriched in ^{13}C (with $\delta^{13}C$ values of –26.5‰ to –23‰) than type I kerogens, which typically have $\delta^{13}C$ values of –27‰ to –29.5‰ (Huang, 1993). Previous studies

Table 1. Selected Geochemical Parameters for Representative Eocene Source Rocks from the Beibuwan Basin.

Sample No.	Formation	Depth (m [ft])	TOC (%)	Pr/Ph	Ts/Tm	Ol/C_{30}H	Ga/C_{30}	C_{27} (%)	C_{28} (%)	C_{29} (%)	C_{30}-4MSI	C_{29}R/(C_{30}-4MST + C_{27}R)	C_{29} 20S/(20S + 20R)	Depositional facies
WZ111-1R1	LS-1	2884–2888 (9462–9476)	2.19	2.34	3.54	0.10	0.07	52	11	37	1.48	0.29	0.29	Shallow lake
WZ111-1R2	LS-1	2928 (9607)	2.60	2.19	4.25	0.12	0.05	56	9	35	0.93	0.26	0.58	Shallow lake
WZ122N-1R1	LS-1	2835–2840 (9302–9318)	4.02	2.88	1.57	0.06	0.07	48	8	44	1.68	0.29	0.28	Shallow lake
WZ122-2R1	LS-2	2480 (8137)	2.41	3.89	1.30	0.06	0.06	39	15	47	1.07	0.40	0.37	Shallow lake
WZ122-2R2	LS-2	2798–2800 (9180–9187)	6.11	1.64	1.64	0.07	0.05	34	14	51	3.75	0.12	0.51	Medium–deep lake
WZ122-2R3	LS-2	2788–2790 (9147–9154)	6.46	1.56	1.43	0.06	0.05	35	13	52	3.88	0.11	0.53	Medium–deep lake
WZ122-2R4	LS-2	2764–2766 (9069–9075)	7.88	1.83	1.28	0.05	0.05	37	15	48	3.12	0.17	0.39	Medium–deep lake
WZ122-2R5	LS-3	2832–2834 (9292–9298)	3.26	1.77	1.37	0.08	0.07	34	14	51	2.61	0.19	0.40	Medium–deep lake
WZ1211-7R1	LS-2	2538–2540 (8327–8334)	8.56	3.52	1.21	0.04	0.02	53	13	34	5.19	0.06	0.68	Medium–deep lake
WZ1211-7R2	LS-2	2558–2560 (8393–8399)	5.53	2.29	0.96	0.06	0.03	43	15	42	7.64	0.04	0.66	Medium–deep lake
WS172-2R1	LS-2	2140–2145 (7021–7038)	5.66	1.66	0.41	0.02	0.02	42	11	47	1.48	0.38	0.14	Medium–deep lake
WS172-2R2	LS-2	2280–2285 (7481–7497)	14.85	3.06	0.46	0.02	0.03	37	14	49	4.32	0.15	0.25	Medium–deep lake
WS172-2R3	LS-2	2250 (7382)	5.51	2.20	0.52	0.02	0.03	42	14	44	3.15	0.19	0.25	Medium–deep lake
WS172-2R4	LS-3	2518–2520 (8262–8268)	2.12	2.41	1.09	0.06	0.06	38	14	48	1.04	0.48	0.21	Shallow lake
WZ118-1R1	LS-3	3392–3394 (11,129–11,136)	0.80	1.76	2.19	0.09	0.06	36	19	45	1.18	0.31	0.52	Shallow lake
WZ118-1R2	LS-3	3312 (10,867)	2.20	2.04	1.96	0.10	0.08	37	22	41	1.21	0.27	0.56	Shallow lake

Abbreviations: C_{27}, C_{28}, and C_{29} (%) = relative percentage of C_{27}, C_{28}, and C_{29} steranes within the C_{27}–C_{29} steranes (20R); C_{29}20S/(20S + 20R) = 20S/(20S + 20R) ratio for αααα-C_{29} steranes; C_{29}R/(C_{30}-4MST + C_{27}R) = C_{29} steranes (20R)/(C_{29} steranes [20R] + C_{30} 4-methylsteranes), calculated from the mass-to-charge ratio (*m*/*z*) 217 mass fragmentograms; C_{30}4-MST = C_{30} 4-methylsteranes; C_{30}-4MSI = ratio of C_{30} 4-methylsteranes to C_{29} regular steranes (20S + 20R); Ga/C_{30} = gammacerane/C_{30}-α β hopane ratio; LS-1 = upper member of the Liushagang Formation; LS-2 = middle member of the Liushagang Formation; LS-3 = lower member of the Liushagang Formation; Ol/C_{30}H = oleanane/C_{30}-α β hopane ratio, calculated from the *m*/*z* 191 mass fragmentograms; Ph = phytane; Pr = pristane; TOC = total organic carbon; Ts/Tm = 18α-trisnorhopane/17α-trisnorhopane; WZ = Weizhou.

illustrated that the abnormal stable carbon isotopic values for type I kerogens are probably related to some submerged aquatic plants whose stable carbon isotopes are isotopically heavy because of the composition of dissolved bicarbonates (Smith and Epstein, 1971; Michael and Livingstone, 1989; Huang, 1993). These aquatic algae or plants use the C3 photosynthetic pathway, and some of them have highly variable and notable ^{13}C-enriched compositions in comparison with terrigenous C3 plants (Fry and Sherr, 1984). For example, the Ibis mudstones in Victoria Lake, East Africa, contain organic matter dominated by C3 aquatic algae with relatively heavy δ^{13}C values between –22.7‰ and –21.16‰ (Michael and Livingstone, 1989). Thus, the relatively heavy δ^{13}C values observed for the kerogens from the medium–deep lake facies in the Liushagang Formation may be attributed to the significant incorporation of specific types of aquatic plant organisms into the kerogens.

Source Rock Potential

The LS-2 shales from the first type of organic facies are organic-rich and exhibit TOC contents ranging from 0.56 to 15.67 wt. % with an average of 3.1 wt. %, and 75% of the samples having TOC values ranging from 1 to 8 wt. % (Figure 10). Most samples from the medium–deep lake facies have Rock-Eval pyrolytic yields (S_1 + S_2) greater than 6 mg hydrocarbons (HC)/g rock with an average of 12.62 mg HC/g rock and hydrogen index (HI) values in the range of 300–700 mg HC/g TOC, and fall into the type I–II_1 kerogen (Figure 6), which is consistent with the maceral observation of their kerogens and illustrates they are strongly oil-prone source rocks. Basin modeling results show that the oils generated by the LS-2 medium–deep lake facies account for approximately 70% of the resources in the two subbasins (Wang et al., 2014).

The LS-1 and LS-3 shale samples from the shallow lake organic facies have TOC contents ranging from 0.35 to 4.73 wt. %. Greater than 50% of the analyzed samples have TOC contents in the range of 1–4 wt. % (Figure 10). The Rock-Eval pyrolytic yields (S_1 + S_2) are from 0.22 to 16.05 mg HC/g rock with an average value of 4.2 mg HC/g rock. The HI values for these samples largely range between 250 and 500 mg HC/g TOC (Figure 6), approximately 200 mg HC/g TOC less than those of the shales from the LS-2 algae-dominated organic facies. The organic matter in most of the LS-1 and LS-3 samples is dominated by type II_1–II_2 kerogens, with a small amount of type I kerogen. This indicates that the source rocks from shallow lake facies have moderate oil generation potential.

Maturation history calibrated with measured vitrinite reflectance (R_o) indicates that the LS entered the threshold of oil generation at a burial depth of approximately 2500 m (8202 ft) (Figure 11A). Results of one-dimensional basin modeling using Schlumberger's PetroMod one-dimensional software (version 11.3) show that oil generation from the LS-3 source rocks close to the central area of the Weixinan Sag began as early as late Eocene and reached peak oil generation during the late Oligocene to Miocene (Figure 11A). The middle part of LS-2 source rocks, largely medium–deep lake source facies, entered maturation threshold ($R_o \approx 0.6\%$) around the middle Oligocene, and the main stage of oil generation occurred during the late Oligocene to

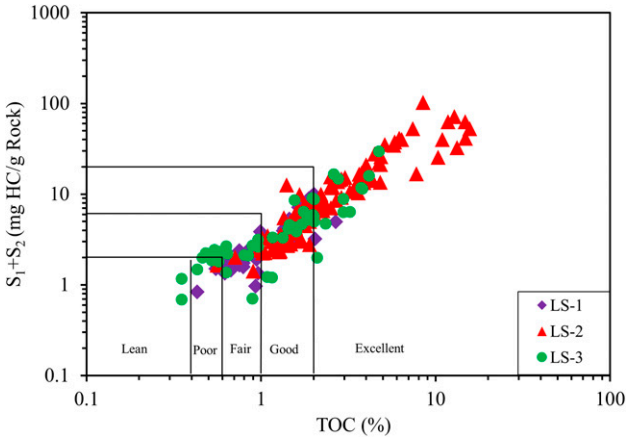

Figure 10. Crossplot of total organic carbon (TOC) vs. Rock-Eval S_1 (free hydrocarbons present in the sample) + S_2 (generative hydrocarbons of the sample) values for the potential source rocks in the Liushagang Formation. HC = hydrocarbons; LS-1 = upper member of the Liushagang Formation; LS-2 = middle member of the Liushagang Formation; LS-3 = lower member of the Liushagang Formation.

Pliocene (Figure 11A), thus providing a favorable hydrocarbon source for late-formed traps in the Weizhou and Jiaowei Formations during the Oligocene and middle Miocene, respectively (Wang et al., 2014). The LS-1 source rocks are developed widely both in the Weixinan and Wushi subbasins, and most of them are buried at a depth range of 1700–3300 m (5577–10,827 ft), with R_o values between 0.3% and 1.0%. Because source rocks located on the slopes of the two sags have a relatively low thermal maturity (Figure 11B), only the LS-1 source rocks in the central parts of the sags have entered the main stage of oil generation (Figure 11A).

Paleodepositional Environment and Productivity

As mentioned above, the Liushagang lacustrine source rocks show significant variability in the distribution of organic facies with varying hydrocarbon generation potentials. Such variation in organic facies among lacustrine source rocks is strongly related to both primary productivity and organic matter preservation, two processes that are linked to the depositional conditions of different lake types (Katz, 1995a; Carroll and Bohacs, 2001). Therefore, a more detailed knowledge of the depositional conditions in the

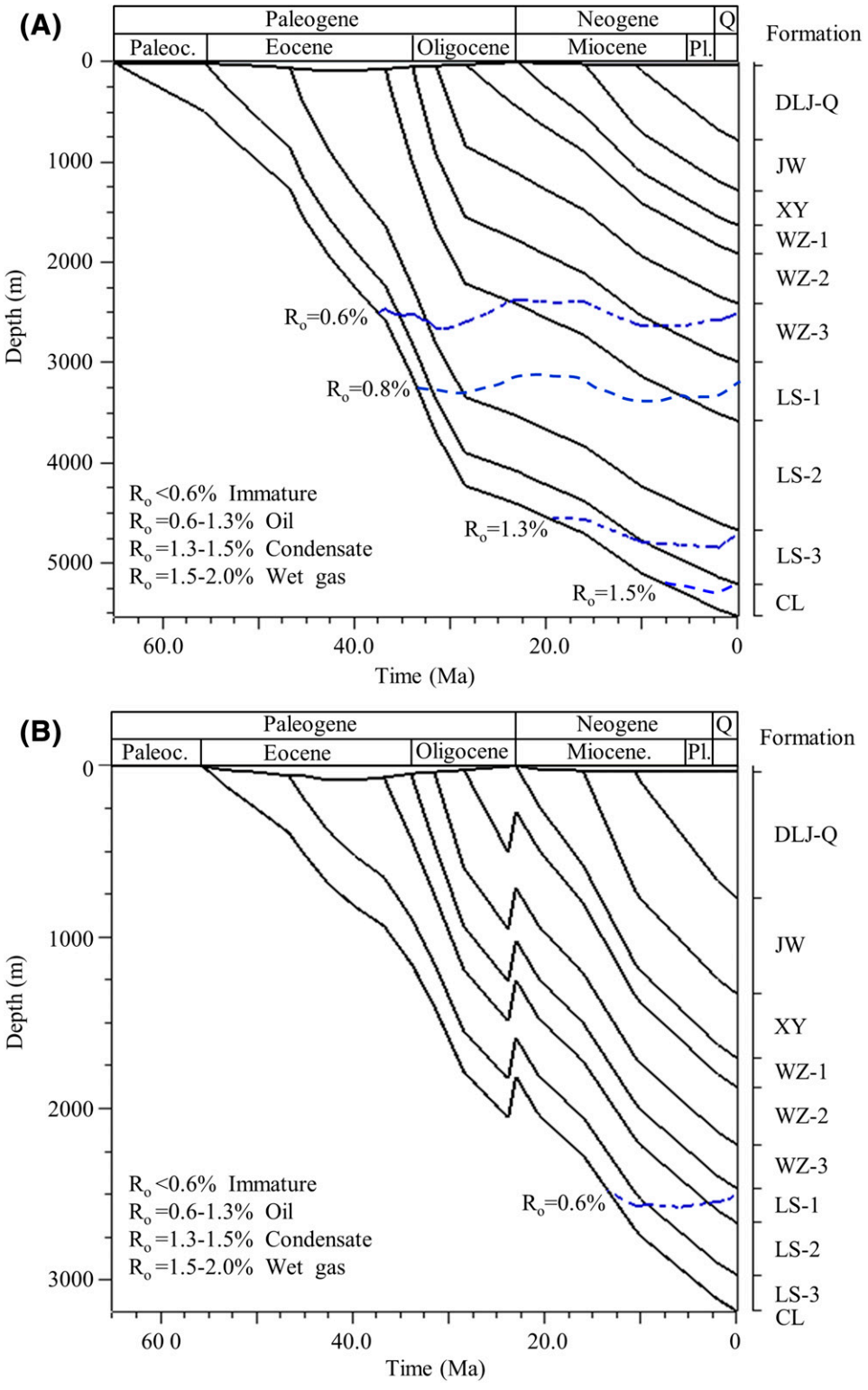

Figure 11. Burial history curves for source rocks (A) near the depocenters and (B) on the slope of the subbasin. The locations of the wells used for this modeling are shown in Figure 1B. Oil window is defined as vitrinite reflectance (R_o) = 0.6%–1.3%. Formation names: CL = Changliu; DLJ = Dengliujiao; JW = Jiaowei; LS-1 = upper member of the Liushagang Formation; LS-2 = middle member of the Liushagang Formation; LS-3 = lower member of the Liushagang Formation; WZ-1 = Upper Weizhou Formation; WZ-2 = Middle Weizhou Formation; WZ-3 = Lower Weizhou Formation; XY = Xiayang. Geological time abbreviations: Paleoc. = Paleocene; Pl. = Pliocene; Q = Quaternary.

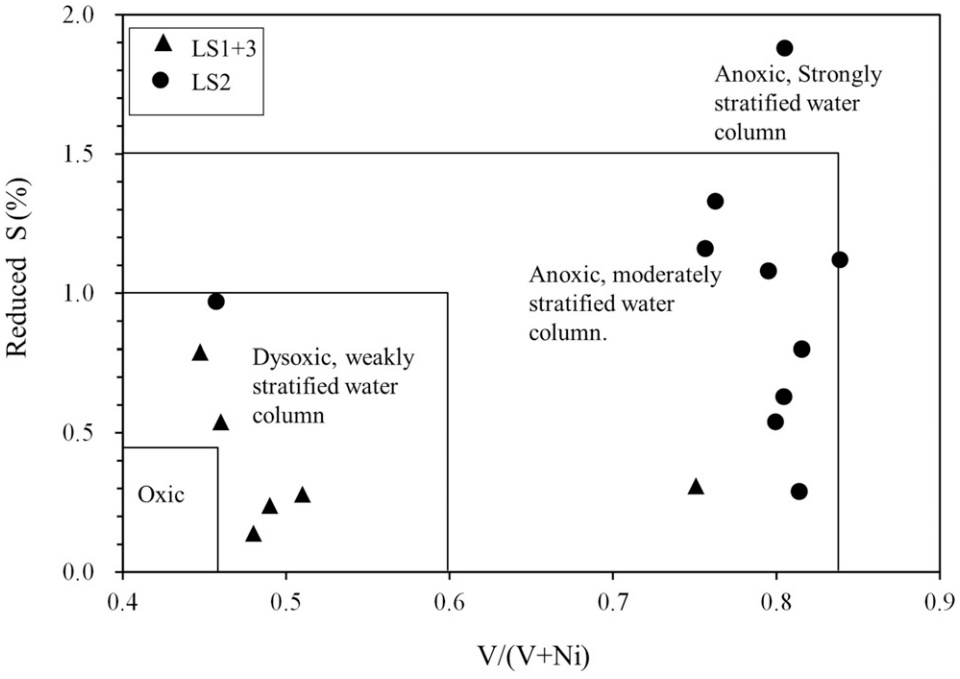

Figure 12. Relationship of V/(V + Ni) to reduced S (S^{-2}) for shale samples from the Liushagang Formation in Weixinan and Wushi subbasins, showing the weakly to moderately stratified water columns of Weixinan and Wushi paleolakes. The boundary lines of V/(V + Ni) are taken from Hatch and Leventhal (1992). LS-1+3 = upper and lower members of the Liushagang Formation; LS-2 = middle member of the Liushagang Formation.

paleolakes during the formation of organic-rich mudstones in the Weixianan and Wushi subbasins is quite important to better understanding the distribution of different organic facies within the LS and their hydrocarbon potentials.

Water Column Stratification

The mudstones in LS-2 member have been interpreted to be deposited in freshwater lake environments with a stratified water column, as evidenced by diagnostic biomarkers and palynological and trace element data. Gammacerane (Ga), a marker of water salinity and water stratification (Sinninghe Damsté et al., 1995; Peters et al., 2005), in the LS-2 mudstones are generally low, with Ga/C_{30}H ratios in the range of 0.02–0.07. Both the low relative abundance of extended homohopanes (>C_{31}) and small amounts of gammacerane suggest a freshwater depositional environment for these organic-rich shales. This is also supported by the presence of certain alginites in several samples that display a similar morphology to the freshwater alga *Botryococcus* (Figure 4C). Nevertheless, brackish water may also exist in the lakes at times, which is evidenced by the minor amount of nonmarine dinoflagellates (such as *Bosedinia*) that compose approximately 3%–10% of total particle abundances (Figure 5).

It is noteworthy that the paleolakes in the Weixinan and Wushi subbasins were located in the subtropical zones, and seasonal variation in air temperature during Eocene was not significant (Li, 1994; Zhu, 2009). This inference is supported by the abundant *Quercoidites* and *Cupuliforoipollenites* found in the LS mudstones (Li,

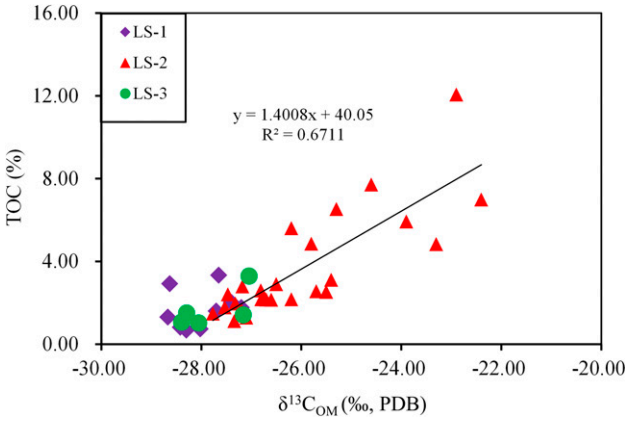

Figure 13. Crossplot of the carbon isotopic composition of kerogen ($\delta^{13}C_{OM}$) vs. total organic carbon (TOC). The $\delta^{13}C_{OM}$values show a positive correlation with wt. % TOC for the middle member of the Liushagang Formation (LS-2) samples from the medium–deep lake facies, indicating an organic productivity control on organic carbon deposition (Curiale and Gibling, 1994). LS-1 = upper member of the Liushagang Formation; LS-3 = lower member of the Liushagang Formation; OM = organic matter; PDB = Peedee belemnite.

Table 2. Basic Data for Representative Oil Samples from the Beibuwan Basin

Sample No.	Formation	Depth (m [ft])	Density (g/cm^3)	Pour point (^oC)	Viscosity (mm^2/s at 50 ^oC)	Sulfur (%)	Wax (%)	Asphaltene (%)	Resin (%)
WZ128-1D3	JW	974–988 (3196–3242)	0.9146	8	70.50	0.28	8.78	5.91	12.02
WS15-1M	XY	1230 (4036)	0.8482	nd	6.99	0.13	1.39	2.84	4.18
WZ68-3M	WZ	2181 (7156)	0.8887	42	396.40	0.29	33.73	8.01	11.57
WZ69-3D2	WZ	2459–2473 (8068–8114)	0.8900	42	nd	0.30	20.36	8.87	14.32
WZ69-3D1	WZ	2582–2618 (8472–8590)	0.8974	45	nd	0.34	23.59	6.27	16.44
WZ69-1D4	WZ	2376–2382 (7796–7815)	0.8904	37	nd	0.31	11.17	7.75	19.38
WZ69-1D3	WZ	2498-2530 (8196–8301)	0.8899	37	nd	0.33	20.35	5.39	20.98
WZ69-1D2	WZ	2923–2935 (9590–9630)	0.8893	40	nd	0.32	21.37	5.79	18.80
WZ121-4D4	WZ	2616-2626 (8583–8616)	0.8441	30	11.93	0.14	15.82	4.65	4.32
WZ610-1D2	WZ	2368–2375 (7769–7792)	0.8374	nd	24.17	0.14	14.65	1.46	6.88
WZ68-1D2	WZ	2351–2357 (7714–7733)	0.8454	33	11.70	0.14	16.59	5.54	5.64
WZ68-1D1	LS-1	2884–2917 (9462–9571)	0.8514	33	10.26	0.19	17.73	3.18	4.85
WZ121-4D2	LS-1	2780–2786 (9121–9141)	0.8235	24	4.51	0.10	12.44	1.44	2.40
WZ121-4D1	LS-1	2810–2847 (9220–9341)	0.8354	27	6.11	0.13	13.25	1.27	4.52
WZ122-1D4	LS-2	2665–2707 (8744–8882)	0.8677	30	16.55	0.12	16.17	4.33	7.42
WZ122-3M	LS-2	2916 (9567)	0.8437	33	nd	0.10	15.7	0.29	3.26
WZ1211-1D1	LS-2	2534.5 (8316)	0.8306	30	4.44	0.09	14.30	0.93	3.72
WZ1211-1D2	LS-2	2577 (8455)	0.8316	30	4.69	0.08	17.50	0.52	4.38
WZ1211-2M1	LS-2	2308 (7573)	0.8311	30	4.88	0.09	13.10	4.33	0.78
WZ1211-2M2	LS-2	2320.5 (7614)	0.8326	33	5.51	0.08	19.50	1.07	4.50
WZ1211-3D2	LS-2	2043–2064 (6703–6772)	0.8505	30	6.73	0.11	14.30	1.69	3.23
WZ1211-3M	LS-2	2048 (6719)	0.8656	33	15.68	0.16	22.60	1.32	5.65

(*continued*)

Table 2. Continued

Sample No.	Formation	Depth (m [ft])	Density (g/cm^3)	Pour point (^{o}C)	Viscosity (mm^2/s at 50 ^{o}C)	Sulfur (%)	Wax (%)	Asphaltene (%)	Resin (%)
WZ1211-4M	LS-2	2151.5 (7059)	0.8567	36	7.40	0.13	14.40	1.46	5.83
WZ1211-6M	LS-2	2189.5 (7184)	0.8781	39	24.31	0.16	7.70	2.71	3.59
WS172-7M	LS-2	1615 (5299)	0.9113	15	nd	0.18	6.79	3.85	9.19
WZ103-30D1	LS-3	2208–2220 (7244–7284)	0.8657	38	25.72	0.21	25.81	1.83	13.01
WZ114N-1D1	LS-3	2592–2629 (8504–8626)	0.7582	2	1.06	0.02	nd	0.30	0.73
WZ1211-3D1	LS-3	2211–2221 (7254–7287)	0.8345	36	4.53	0.11	15.30	1.00	2.62
WZ122-1D1	LS-3	2913–2988 (9558–9804)	0.8890	38	52.64	0.08	24.62	3.52	8.90
WZ118-1D2	LS-3	3104–3270 (10,184–10,729)	0.8363	30	4.46	0.08	10.94	1.66	1.45
WZ118-1D1	LS-3	3288–3383 (10,788–11,100)	0.8385	30	5.23	0.10	11.42	1.86	2.22
WZ111-1D5	LS-3	2681–2687 (8796–8816)	0.8914	38	96.78	0.31	24.70	5.40	11.28
WS162-1M	LS-3	1308 (4292)	0.9565	-3	nd	0.20	1.97	11.70	7.44
WS172-1M	LS-3	2627.2 (8620)	0.8164	36	3.76	0.07	11.60	1.10	1.83
WS172-1D2	LS-3	2619–2646 (8593–8682)	0.8046	33	3.58	0.05	13.60	1.98	0.60
WS172-1D1	LS-3	2634–2646 (8642–8682)	0.8062	33	3.75	0.04	13.60	2.14	0.66
WZ61-1D2	C	1967–2052 (6454–6733)	0.8246	29	5.38	0.02	20.54	0.46	3.05
WZ123-1D1	C	1409–1421 (4623–4662)	0.8554	30	9.97	0.10	18.85	3.96	5.75

Abbreviations: C = Carboniferous; JW = Jiaowei; LS-1 = upper member of the Liushagang Formation; LS-2 = middle member of the Liushagang Formation; LS-3 = lower member of the Liushagang Formation; nd = not determined; WS = Wushi; WZ = Weizhou; XY = Xiayang.

1994), which typically thrive in warm and wet climates (Li, 1994; Wang et al., 2005). As a result, the warm and low-density surface water in the lake permanently overlies the cool and deep water, resulting in a stable water stratification and following bottom-water anoxia (Zhu, 2009).The stratification of lake water can be enhanced by an influx of fresh water from adjacent rivers, which suppresses water circulation further (Yang, 1995; Zhu, 2009). At the same time, the oxygen in the water is consumed by organic detritus showering from the epilimnion but cannot be replenished at a sufficient rate to the sluggish and stagnant deep water because of stratification, promoting the development of anoxic bottom-water further.

Early studies show that $\delta^{13}C_{OM}$ (organic matter) values are indicators of both productivity fluctuation (directly) in the surface water and preservation (indirectly) near the water–sediment interface and reflect the extents of water column stratification and anoxia (Curiale and Gibling, 1994). The relatively heavy

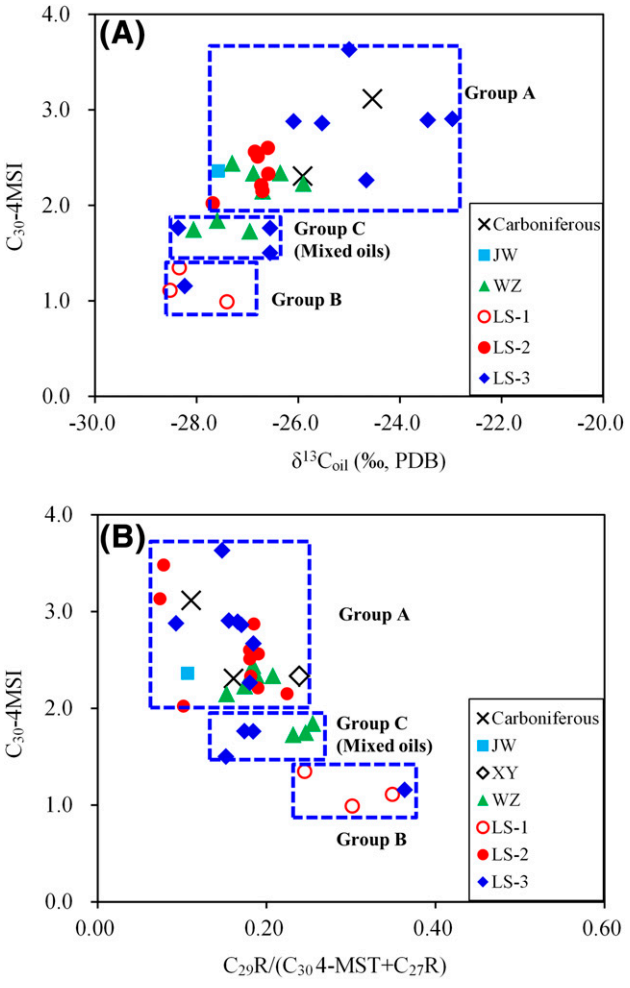

Figure 14. Crossplots of ratio of C_{30} 4-methylsteranes to C_{29} regular steranes (20R + 20S) (C_{30}-4MSI) vs. (A) whole oil $\delta^{13}C$ values and (B) ratios of $C_{29}R/(C_{30}\text{-4MST} + C_{27}R)$, showing three different oil groups. High C_{30}-4MSI values indicate strong algal input; $C_{29}R/(C_{30}\text{-4MST} + C_{27}R) = C_{29}$ ααα 20R sterane/(C_{27} ααα 20R sterane + C_{30} 4-methylsteranes), calculated from the mass-to-charge ratio 217 mass chromatograms, with high $C_{29}R/(C_{30}\text{-4MST} + C_{27}R)$ ratios reflecting an increased land plant input. JW = Jiaowei; LS-1 = upper member of the Liushagang Formation; LS-2 = middle member of the Liushagang Formation; LS-3 = lower member of the Liushagang Formation; PDB = Peedee belemnite; WZ = Weizhou; XY = Xiayang.

$\delta^{13}C_{OM}$ values (–22.4‰ to –27.5‰) and abundant AOM, along with the absence of any evidence of bottom-dwelling fauna in the strongly laminated mudstones from the LS-2 member, suggest that anoxic conditions prevailed near the sediment–water interface. This interpretation is also supported by the available trace element data. In oxic settings, V is relatively insoluble in water, resulting in low V/(V + Ni) ratios (Hatch and Leventhal, 1992). In contrast, it becomes more soluble in reducing conditions and can dissipate into the water column (Hatch and Leventhal, 1992). Thus, high V/(V + Ni) ratios (0.84–0.89) indicate the presence of H_2S in a strongly stratified water column; intermediate V/(V + Ni) ratios (0.60–0.82) represent a moderately stratified anoxic water column; and low V/(V + Ni) ratios (0.46–0.60) reflect a weakly stratified, dysoxic water column (Hatch and Leventhal, 1992). As shown in Figure 12, the V/(V + Ni) ratios of shale samples from the LS-2 member range from 0.74 to 0.84, denoting an moderately stratified, anoxic water column. This contracts with the data from the LS-1 and LS-3 source rocks that appear to have been deposited in a weakly stratified, dysoxic–anoxic water column, with V/(V + Ni) ratios in the range of 0.47–0.52 (Figure 12).

Redox Conditions

The pristane/phytane (Pr/Ph) ratio is a commonly used parameter for the study of oxic/anoxic conditions (Didyk et al., 1978; ten Haven et al., 1987). Low Pr/Ph values (<1 or 0.8) indicate anoxic environments, whereas high values (>3) reflect oxic conditions of sedimentation (Peters et al., 2005). As shown in Table 1, Pr/Ph ratios range from 1.5 to 3 throughout the Liushagang Formation, normally interpreted as suboxic conditions. No significant change in Pr/Ph ratios was observed throughout the data profile of LS. This seems to indicate a constant redox conditions with the evolution of organic facies; however, the decreased TOC and AOM contents from the LS-2 to LS-1 members (Figure 3) do reflect the change of their depositional environments. In effect, the Pr/Ph ratios alone might be inadequate to accurately define the redox conditions because the preservation of Pr and Ph is also affected by sulfurization, thermal maturity, and the changes in sources of organic matter besides the redox conditions (Didyk et al., 1978; ten Haven et al., 1987; Peters et al., 2005).

The maceral assemblages of kerogens can reflect the composition and preservation of organic matter in shales (Michael and Livingstone, 1989). Distinct from both LS-1 and LS-3 members, the LS-2 member is characterized by abrupt abundance AOM (up to 70%–80%) in the organic-rich interval (Figure 3), corresponding to the relatively abundant algal fossil particles as shown in Figure 5. Therefore, the occurrence of the abundant AOM derived from the

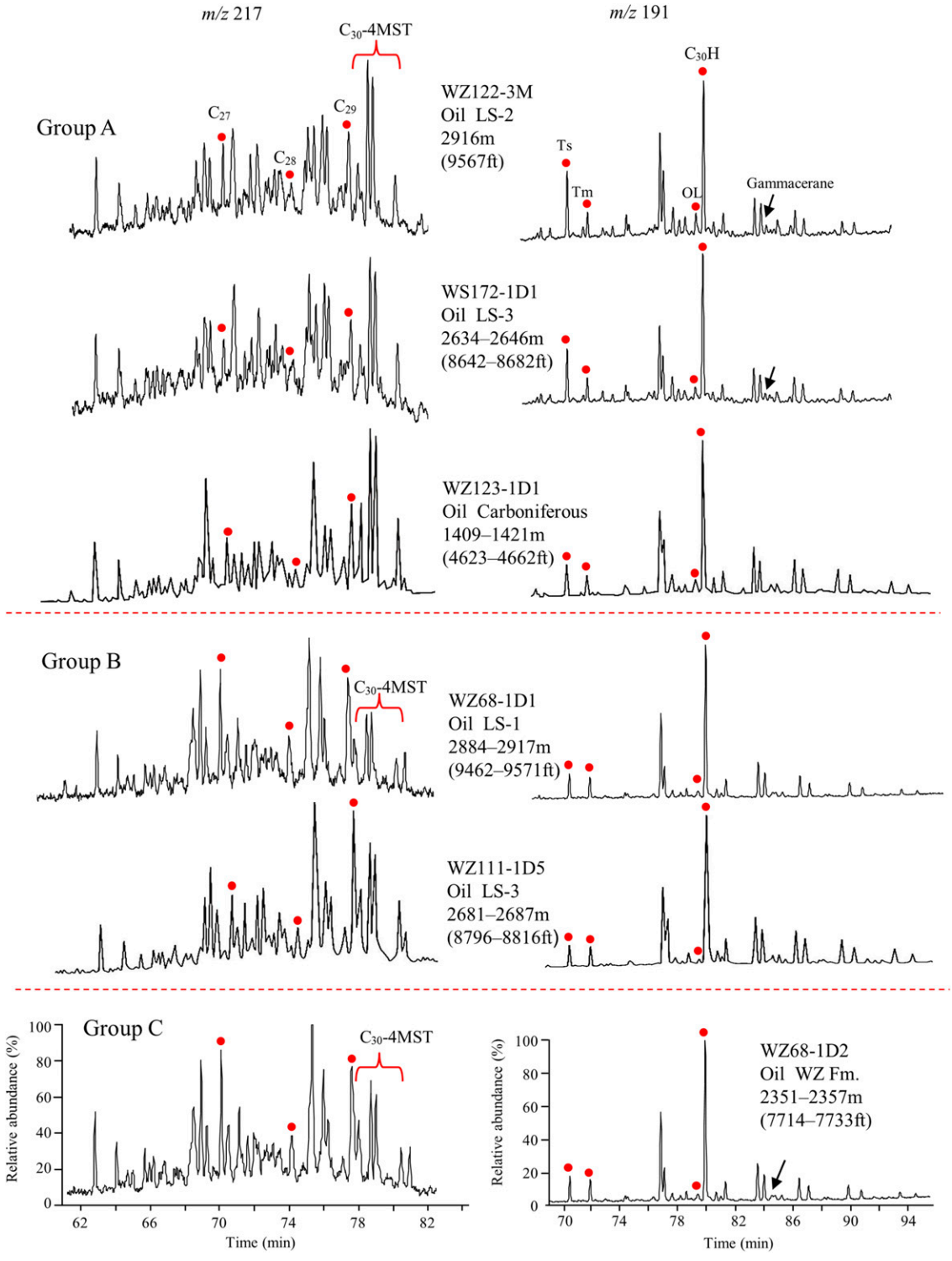

Figure 15. Mass-to-charge ratio (*m*/*z*) 191, 217, and 191 mass chromatograms of three groups of oils from the Weixinan and Wushi subbasins. C_{27}, C_{28}, and C_{29} = C_{27}, C_{28}, and C_{29} ααα 20R steranes; C_{30}-4MST = C_{30} 4-methylsteranes; $C_{30}H$ = C_{30} αβ hopane; Fm. = Formation; LS-1 = upper member of the Liushagang Formation; LS-2 = middle member of the Liushagang Formation; LS-3 = lower member of the Liushagang Formation; OL = oleanane; Tm = 17α-trisnorhopane; Ts = 18α-trisnorhopane; WS = Wushi; WZ = Weizhou.

Table 3. Selected Geochemical Parameters for Representative Oil Samples from the Beibuwan Basin

Sample No.	Formation	Depth (m [ft])	Pr/Ph	Ts/Tm	Ol/C_{30}H	Ga/C_{30}	C_{27} (%)	C_{28}(%)	C_{29}(%)	C_{30}-4MSI	C_{29}R/ (C_{30}-4MST + C_{27}R)	C_{29} 20S/ (20S + 20R)	$\delta^{13}C_{oil}$ (‰)	Genetic Type
WZ128-1D3	JW	974–988 (3196–3242)	1.85	1.61	0.09	0.021	50	19	31	2.36	0.11	0.70	−27.57	A
WS15-1M	XY	1230 (4036)	2.12	1.20	0.06	0.029	39	15	47	2.33	0.24	0.47	nd.	A
WZ68-3M	WZ	2181 (7156)	1.76	0.99	0.02	0.003	36	14	50	2.44	0.18	0.48	−27.30	A
WZ69-3D2	WZ	2459–2473 (8068–8114)	1.76	0.90	0.03	0.016	32	15	53	2.23	0.17	0.62	−25.90	A
WZ69-3D1	WZ	2582–2618 (8472–8590)	1.68	0.68	0.03	0.008	40	14	46	2.15	0.15	0.64	−26.70	A
WZ69-1D4	WZ	2376–2382 (7796–7815)	1.74	0.97	0.02	0.016	35	14	51	2.34	0.21	0.44	−26.88	A
WZ69-1D2	WZ	2923–2935 (9590–9630)	1.64	0.72	0.02	0.008	36	15	49	2.34	0.19	0.49	−26.35	A
WZ69-1D3	WZ	2498-2530 (8196–8301)	1.79	0.68	0.01	0.004	32	11	56	1.84	0.25	0.45	−27.59	C
WZ121-4D4	WZ	2616-2626 (8583–8616)	2.04	1.39	0.04	0.020	35	11	55	1.75	0.25	0.57	−28.06	C
WZ610-1D2	WZ	2368–2375 (7769–7792)	1.97	1.12	0.04	0.030	47	12	41	1.73	0.23	0.45	−26.95	C
WZ68-1D2	WZ	2351–2357 (7714–7733)	2.12	1.50	0.04	0.016	49	9	42	1.65	0.24	0.46	nd.	C
WZ68-1D1	LS-1	2884–2917 (9462–9571)	2.18	1.07	0.04	0.016	48	8	45	0.99	0.30	0.56	−27.40	B
WZ121-4D2	LS-1	2780–2786 (9121–9141)	2.04	1.67	0.05	0.036	32	19	49	1.35	0.25	0.61	−28.34	B
WZ121-4D1	LS-1	2810–2847 (9220–9341)	2.11	1.40	0.04	0.028	37	11	53	1.11	0.35	0.49	−28.52	B
WZ122-1D4	LS-2	2665–2707 (8744–8882)	2.43	2.22	0.04	0.007	41	21	37	2.02	0.11	0.78	−27.68	A
WZ122-3M	LS-2	2916 (9567)	2.00	2.63	0.14	0.010	36	15	49	2.80	0.18	0.45	nd.	A
WZ1211-1D1	LS-2	2534.5 (8316)	2.40	2.41	0.06	0.030	27	5	68	2.60	0.18	0.50	−26.61	A
WZ1211-1D2	LS-2	2577 (8455)	2.34	2.65	0.07	0.026	26	8	66	2.33	0.18	0.57	−26.58	A
WZ1211-2M1	LS-2	2308 (7573)	2.52	2.12	0.06	0.024	31	6	62	2.15	0.22	0.50	−26.73	A
WZ1211-2M2	LS-2	2320.5 (7614)	2.40	2.18	0.06	0.018	36	7	57	2.21	0.19	0.52	−26.73	A
WZ1211-32	LS-2	2043–2064 (6703–6772)	2.38	1.74	0.06	0.014	28	7	65	2.56	0.19	0.47	−26.83	A
WZ1211-3M	LS-2	2048 (6719)	2.47	1.85	0.05	0.018	27	7	66	2.51	0.18	0.51	−26.78	A
WZ1211-4M	LS-2	2151.5 (7059)	2.27	1.91	0.07	0.019	33	31	36	3.48	0.08	0.71	nd.	A
WZ1211-6M	LS-2	2189.5 (7184)	2.82	1.98	0.06	0.025	45	19	37	3.13	0.07	0.75	nd.	A
WS172-7M	LS-2	1615 (5299)	2.39	1.33	0.05	0.034	31	12	56	2.87	0.19	0.41	nd.	A

(*continued*)

Table 3. Continued

Sample No.	Formation	Depth (m [ft])	Pr/ Ph	Ts/ Tm	Ol/ $C_{30}H$	Ga/ C_{30}	C_{27} (%)	C_{28}(%)	C_{29}(%)	C_{30}-4MSI	$C_{29}R$/ (C_{30}-4MST + $C_{27}R$)	C_{29} 20S/ (20S + 20R)	$\delta^{13}C_{oil}$ (‰)	Genetic Type
WZ103-30D1	LS-3	2208–2220 (7244–7284)	1.94	1.00	0.10	0.054	29	16	55	2.26	0.18	0.55	–24.66	A
WZ114N-1D1	LS-3	2592–2629 (8504–8626)	2.50	1.77	0.24	0.085	46	18	35	2.88	0.09	0.70	–26.09	A
WZ1211-3D1	LS-3	2211–2221 (7254–7287)	2.52	1.07	0.07	0.022	37	10	54	3.63	0.15	0.41	–25.00	A
WZ122-1D1	LS-3	2913–2988 (9558–9804)	2.40	1.55	0.03	0.008	29	18	53	1.76	0.17	0.66	–28.36	C
WZ118-1D2	LS-3	3104–3270 (10,184–10,729)	2.48	nd.	0.26	0.001	40	28	32	1.78	0.18	0.53	–26.55	C
WZ118-1D1	LS-3	3288–3383 (10,788–11,100)	2.23	nd.	0.29	0.001	40	23	37	1.50	0.15	0.55	–26.55	C
WZ111-1D5	LS-3	2681–2687 (8796–8816)	2.30	1.14	0.03	0.047	24	13	63	1.16	0.36	0.51	–28.23	B
WS162-1DM	LS-3	1308 (4292)	2.54	1.41	0.14	0.095	40	11	49	2.86	0.17	0.44	–25.53	A
WS172-1DM	LS-3	2627.2 (8620)	2.19	1.59	0.07	0.044	41	14	45	2.67	0.18	0.41	nd.	A
WS172-1D2	LS-3	2619–2646 (8593–8682)	2.27	2.05	0.09	0.052	37	16	47	2.89	0.17	0.45	–23.45	A
WS172-1D1	LS-3	2634–2646 (8642–8682)	2.15	2.18	0.09	0.053	33	20	48	2.90	0.16	0.49	–22.97	A
WZ61-1D2	C	1967–2052 (6454–6733)	2.25	1.81	0.10	0.021	35	15	50	3.11	0.11	0.61	–24.54	A
WZ123-1D1	C	1409–1421 (4623–4662)	2.76	1.46	0.09	0.043	30	22	49	2.31	0.16	0.59	–25.91	A

Abbreviations: C = Carboniferous; C_{27}, C_{28}, and C_{29} (%) = relative percentage of C_{27}, C_{28}, and C_{29} steranes within the C_{27}–C_{29} steranes (20R); C_{29}20S/(20S + 20R) = 20S/(20S + 20R) ratio for ααα-C_{29} steranes; $C_{29}R/(C_{30}\text{-4MST} + C_{27}R)$ = C_{29} steranes (20R)/(C_{29} steranes [20R] + C_{30} 4-methylsteranes), calculated from the mass-to-charge ratio (*m/z*) 217 mass fragmentograms; C_{30}-4MSI = ratio of C_{30} 4-methylsteranes to C_{29} regular steranes (20S + 20R); Ga/C_{30} = gammacerane/C_{30}-α β hopane ratio; JW = Jiaowei; LS-1 = upper member of the Liushagang Formation; LS-2 = middle member of the Liushagang Formation; LS-3 = lower member of the Liushagang Formation; nd = not determined; $Ol/C_{30}H$ = oleanane/C_{30}-α β hopane ratio, calculated from the *m/z* 191 mass fragmentograms; Ph = phytane; Pr = pristane; Ts/Tm = 18α-trisnorhopane/17α-trisnorhopane; WS = Wushi; WZ = Weizhou; XY = Xiayang.

degradation of alginites in the LS-2 samples implies both high productivity and an oxygen-deficient depositional environment, which, in turn, favors the preservation of organic matter.

Productivity

The carbon isotopic composition of organic matter can be a sensitive indicator that reflects the relative importance of bioproductivity and redox conditions controls on TOC content. Where bioproductivity is important, $\delta^{13}C$ of organic matter correlates positively with TOC (Hollander and McKenzie, 1991; Curiale and Gibling, 1994). In contrast, a negative relationship exists between TOC and $\delta^{13}C$ values of kerogen when TOC is mainly determined by redox conditions (Freeman et al., 1994; Schouten et al., 2000). The $\delta^{13}C$ values for the LS-1 and LS-3 kerogens are generally light (–27.20‰ to –28.67‰), and no strong correlation is observed between $\delta^{13}C$ of kerogens and TOC based on their limited data set and isotopic range. The $\delta^{13}C$ composition of kerogen in the LS-2 samples, however, shows a significant variation, ranging from –22.4‰ to –27.5‰ (Figure 13), and a moderately positive correlation between $\delta^{13}C$ of kerogen and TOC is observed with a coefficient of determination of 0.67. This suggests that the bioproductivity exerted some control on the TOC contents in the LS-2 member.

These geochemical results are consistent with the maceral composition of kerogens isolated from

the LS (Figure 3); for example, large and abundant *Leiosphaeridia* and *Botryococcus* alginites commonly occur in some LS-2 samples (Figure 4A) where the alginate/sporopollen ratios are up to 0.62 (Figure 5), implying an algal bloom (Zhu and Wu, 2004; Huang et al., 2013). These data indicate that the transition from shallow to medium–deep lakes marks an increase in the importance of productivity to organic matter accumulation because a euphotic zone with sufficiently low-energy water dynamics would be more favorably developed in medium–deep lakes than in shallow lakes, thus increasing algal blooms and productivity in medium–deep lake environments (Li, 1994; Zhu and Wu, 2004). In effect, productivity and preservation increase simultaneously in such a circumstance because increased biomass sinking to the water–sediments interface yields a water column depleted in molecular oxygen, generating dysoxic or anoxic conditions and thus allowing the TOC in the LS-2 member sediments to remain near their original high values (Curiale and Gibling, 1994).

Oil Grouping

The physical properties of the oils from the two subbasins are listed in Table 2. They are black to brown in color, with medium to high density (0.7582–0.9565 g/cm^3). Except for a few biodegraded oils, all of the samples are characterized by high wax (up to 33.73%) and low sulfur contents (0.02%–0.34%) (Table 2), showing a typical nonmarine origin (Gransch and Posthuma, 1974). Most of the oils are predominantly composed of saturated hydrocarbons (50%–80%). The discovered oils can be largely classified into three groups based on their geochemical attributes and stable carbon isotopic compositions (Figures 14, 15, Tables 2, 3).

Group A oils include oils from reservoirs in the Xiayang, Jiaowei, and Weizhou Formations, as well as the Carboniferous strata, and some reservoirs within the LS-3, LS-2, and LS-1 members (Tables 2, 3) and are present in the Wushi (WS) 172, Weizhou (WZ) 123, WZ1211, WZ103, and WZ68 oil fields (Figure 16).This group's oils account for the overwhelming bulk of the proven oil reserves in the studied area. The group A oils are distinct from other groups by their high relative abundance of C_{30} 4-methylsteranes, with C_{30}-4MSI values in the range of 2.02–3.63. These oils show a moderate Pr/Ph ratio of 1.64–2.82 and a relatively low oleanane content, with very low gammacerane content. Therefore, the group A oils are most likely derived from source rocks deposited in a medium–deep freshwater environment. The sterane molecular ratios of C_{29}20S/(20S + 20R) for the majority of group A oils are in

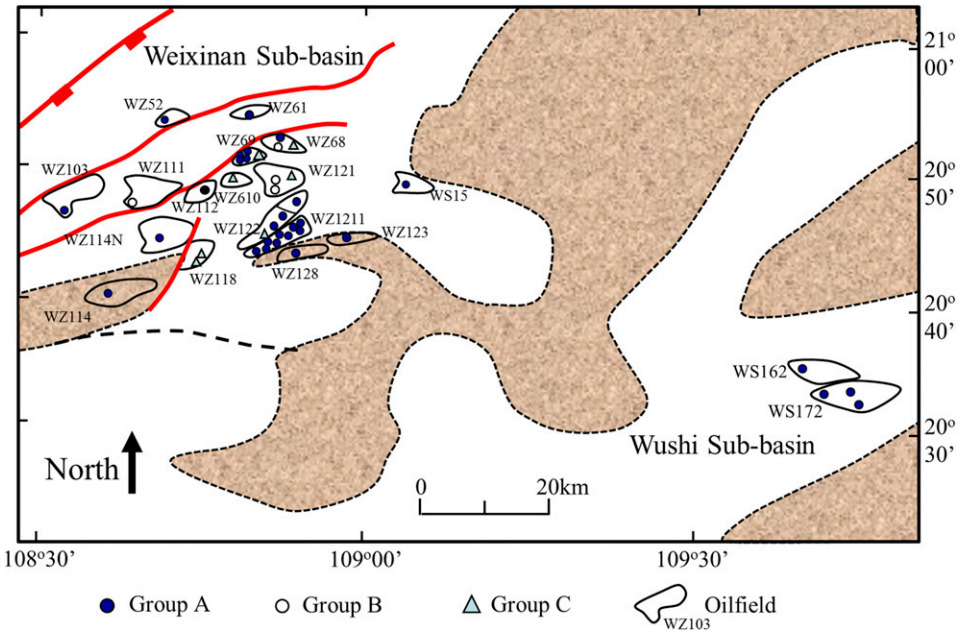

Figure 16. Map showing the distribution of different oil groups in the Weixinan and Wushi subbasins. WZ = Weizhou.

the range of 0.50–0.65, indicating that their source rocks have reached the peak stage of oil generation (Seifert and Moldowan, 1978, 1986). Note that some of the ratios are uncommonly high (up to 0.73), and this might be caused by interference from the presence of the large quantities of C_{30} 4-methylsteranes. These anomalous data provide no reliable information on the real maturity levels of oils (Table 3). All of the oil samples have Ts/Tm (18α-trisnorhopane/17α-trisnorhopane) ratios close to or greater than 1.0 with low moretane content, also indicating they are thermally mature oils (Seifert and Moldowan, 1978, 1986; Peters et al., 2005). Meanwhile the carbon isotopes of this group oils range from –22.97‰ to –27.68‰ with an average value of –24.5‰, approximately 3‰–4‰ heavier than those of group B and C oils (Figure 14, Table 3).

Group B oils are principally encountered in the LS-1 and LS-3 sandstone reservoirs (Figure 16) and are characterized by a relatively low abundance of C_{30} 4-methylsteranes with the C_{30}-4MSI values of 0.99–1.35 and relatively light carbon isotope values (–28.52‰ to –27.4‰) in comparison with group A and C oils (Figures 14, 15, Table 3). Their Pr/Ph ratios are between 2.04 and 2.30, which is not significantly different from the other two groups of oils, but their reduced abundance of C_{30} 4-methylsteranes and lighter carbon isotope values of whole oils indicate that the group B oils are derived from source rocks with probably increased contribution of terrigenous organic matter. This is also supported by the increased values of $C_{29}R/(C_{30}\text{-4MST} + C_{27}R)$, which is defined as the ratio of C_{29} ααα20R sterane to the sum of C_{27} ααα20R sterane and C_{30} 4-methylsteranes and reflects the relative importance of terrigenous input over aquatic organic matter (Goodwin et al., 1988; Peters et al., 2005; Huang et al., 2013).

Group C oils are mainly produced from the sandstone reservoirs in the Weizhou Formation, LS-1, and LS-3 members (Figure 16). It is believed that this group of oils is a mixture of group A and B oils, as discussed below, because they show intermediate biomarker ratios and carbon isotopic values (Figures 14, 15, Table 3). For example, the mixed oils have a moderate abundance of C_{30} 4-methylsteranes with the C_{30}-4MSI of 1.5–1.92. Their ratios of $C_{29}R/(C_{30}\text{-4MST} + C_{27}R)$ range from 0.15 to 0.25, which are larger than those of group B oils but smaller than those of group A oils, thus reflecting inputs of both terrigenous organic matter and aquatic algae. Furthermore, their carbon isotopic values are in the range of –28.36‰ to –26.55‰, falling into the area between group A and B oils.

Oil–Source Correlation

The three groups of oils produced from the Weixinan and Wushi subbasins are derived from two distinct organic facies. The relative abundance of C_{30} 4-methylsteranes and the stable carbon isotopic values have been used as parameters for oil–source correlation here because they are most distinct between the two organic facies in the studied area.

Figure 17 shows *m/z* 191 and 217 mass chromatograms of the two end-member oils (groups A and B) and their corresponding source rocks. High abundances of C_{30} 4-methylsteranes are recognized in both group A oils and medium–deep lake shales from the LS-2 member, indicating their genetic relationship. Noticeably, the WS172-2R2 source rock sample displays relatively low thermal maturity as evidenced from its biomarker signatures (Figure 7), and therefore, the group A oils in WS172 oil field must be derived from more thermally mature medium–deep lake source rocks in the Wushi subbasin.

This biomarker-based oil–source correlation is further supported by $\delta^{13}C$ data, and both the group A oils and their source rocks have the heaviest stable carbon isotopes (Figure 18). It seems that the carbon isotopic fractionation between source rocks and their oils is not as evident as expected; for example, the $\delta^{13}C$ values of the oils should be approximately 1%–2% lighter than those of their kerogens (Clayton, 1991). One reason for this phenomenon is that both the oils and their kerogens vary significantly in $\delta^{13}C$ values, and the $\delta^{13}C$ values for the oils sample may reflect a composite of kerogens with wide-ranging $\delta^{13}C$ values (Figure 18). Curiale and Gibling (1994) illustrated that kerogens with heavier $\delta^{13}C$ values commonly have a greater hydrocarbon potential (hydrogen index), which indicates that the kerogens with heavier $\delta^{13}C$ values may have contributed more to the oils, either group A or B, than the kerogens with lighter $\delta^{13}C$ values. Therefore, our carbon isotope data still provide some genetic relationships between oils and kerogens, though carbon isotope fractionation (approximately 1‰–2‰) between the oils and their

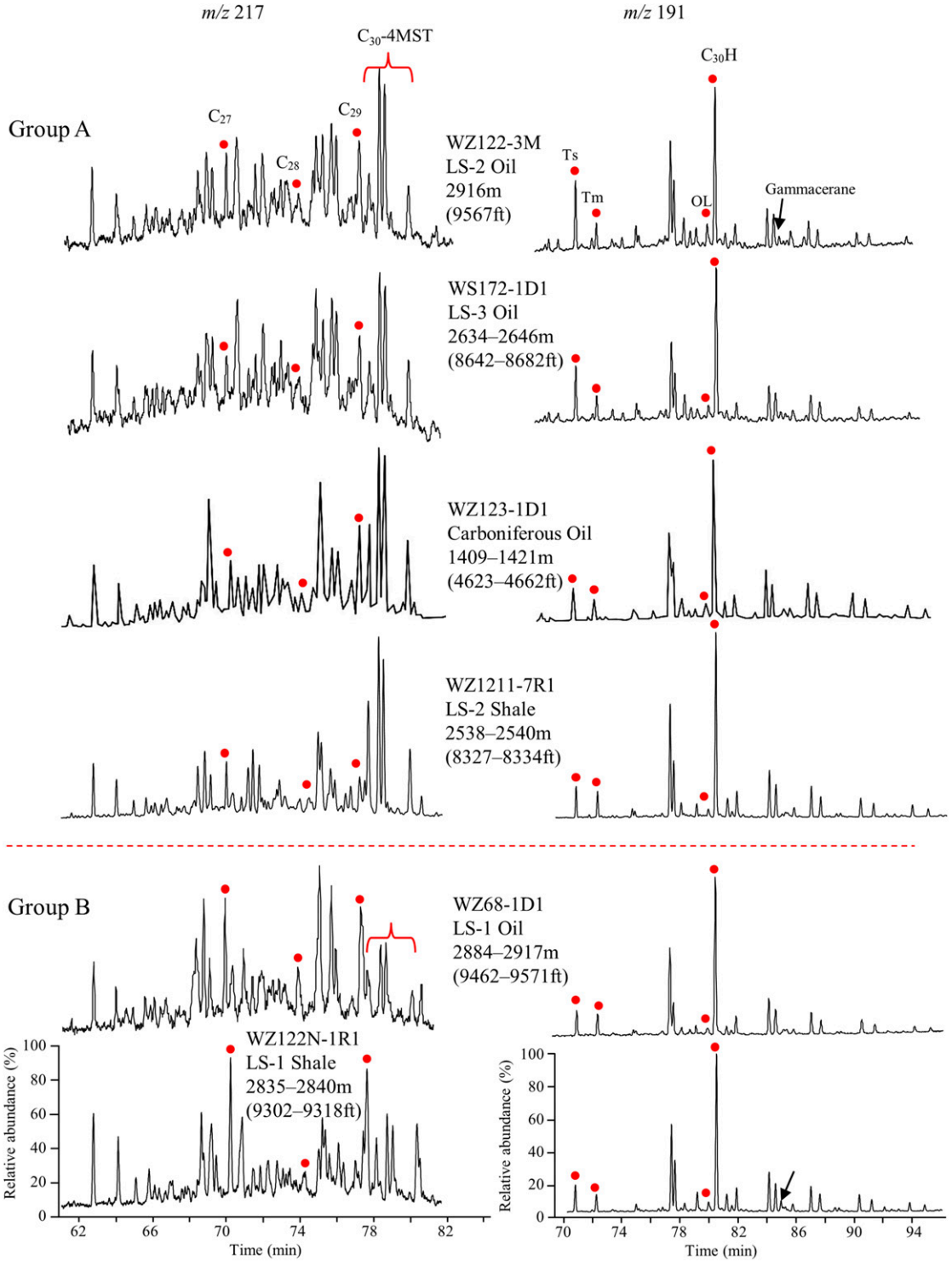

Figure 17. Correlation of the two end-member oils with their source rocks based on distinctive biomarkers of steranes (mass-to-charge ratio [*m/z* 217]) and terpanes (*m/z* 191). C_{27}, C_{28}, and C_{29} = C_{27}, C_{28}, and C_{29} ααα 20R steranes; C_{30}-4MST = C_{30} 4-methylsteranes; C_{30}H= C_{30}αβ hopane; LS-1 = upper member of the Liushagang Formation; LS-2 = middle member of the Liushagang Formation; LS-3 = lower member of the Liushagang Formation; OL = oleanane; Tm = 17α-trisnorhopane; Ts = 18α- trisnorhopane; WZ = Weizhou.

kerogens has been masked by significant variations in carbon isotopes of both oils and kerogens.

Based on the relatively low abundance of C_{30} 4-methylsteranes and lighter carbon isotopic values, group B oils can be correlated to the shallow lake organic facies within the Liushagang Formation, especially within the LS-3 and LS-1 members (Figures 17, 18). In terms of biomarker distribution, the oils in the LS-3 and the LS-1 reservoirs are more possibly derived from the source rocks within the LS-3 and the LS-1 members, respectively (Figure 16). This correlation scheme is quite geologically feasible (see details in the following paragraphs; Figure 19).

On the basis of the conventional fingerprint correlation technique, none of the source rocks analyzed in this study are well matched with group C oils, though several LS rock extracts do have Pr/Ph ratios similar to this group of oils. However, the mixing of group A and B oils can yield oils with such intermediate molecular and isotopic compositions as held by group C oils (Figure 14), indicating a mixed origin of this group oils.

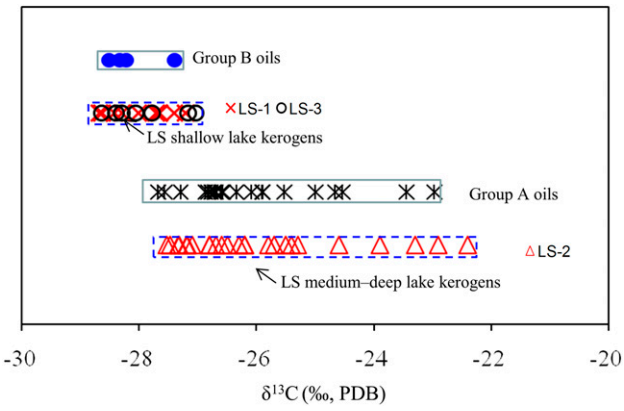

Figure 18. Correlation of the two end-member oils with their kerogens based on their $\delta^{13}C$ values. Note that carbon isotope fractionation between the oils and their kerogen might have been masked by their significant variation in $\delta^{13}C$ values. Actually, kerogens with heavier $\delta^{13}C$ values might have contributed more to the oils than those with lighter $\delta^{13}C$ values because hydrocarbon potential (either total organic carbon or hydrogen index) is positively correlated with $\delta^{13}C$ values (Curiale and Gibling, 1994; see details in text). LS = Liushagang Formation; LS-1 = upper member of the Liushagang Formation; LS-2 = middle member of the Liushagang Formation; LS-3 = lower member of the Liushagang Formation; PDB = Peedee belemnite.

Migration Model and Implications for Petroleum Exploration

Our oil–source evaluation indicates two major effective source rock facies within the Eocene: the LS-1 and LS-3 shallow lake facies and the LS-2 medium–deep lake facies. As discussed above, group B oils, found only in the LS-3 and LS-1 reservoirs, are sourced from shallow lake source rocks in the LS-3 and LS-1 members, respectively, and their restricted distribution suggests a short-distance migration from the nearby source kitchens.

Burial history results show that the LS-1 member is deeply buried only in the depositional centers of the two subbasins where it is thermally mature enough to generate more hydrocarbons than in the slope areas. Additionally, the reservoirs within the LS-1 member are shallowly buried with weak to moderate diagenesis in comparison with reservoirs within the LS-3 member (Liu, 2004), and therefore, they are expected to have good reservoir properties and represent an important target, especially in the central parts of the subbasins.

The group A oils are found within reservoirs ranging in age from Carboniferous to Miocene and are mainly sourced from the medium–deep lake source rocks in the LS-2 member. A close examination of the spatial distribution of both group A and their most possible source rocks reveals that three distinct migration systems might have developed in the two subbasins (Figure 19).

Oil reservoirs within the LS-2 member are related to the first migration system through which the oils likely migrated directly into the reservoirs adjacent LS-2 source rock layers, such as in the WZ122 and WZ1211 oil fields.

The second migration system can be represented by the filling of LS-2-sourced oils into the Oligocene and Miocene sandstone traps. Because these traps are separated from the LS-2 source kitchen by a thick succession of shales in the LS-1 member and Weizhou Formation, these oils might have migrated upward along fractures and faults that developed concurrent with the formation of Oligocene and Miocene traps. All group A oils share similar thermal maturity levels, no matter whether they are located in deep reservoirs (e.g., the WZ122-3M sample with a depth of 2916 m [9567 ft]) or shallow reservoirs (e.g., the WS15-1M sample with a depth of

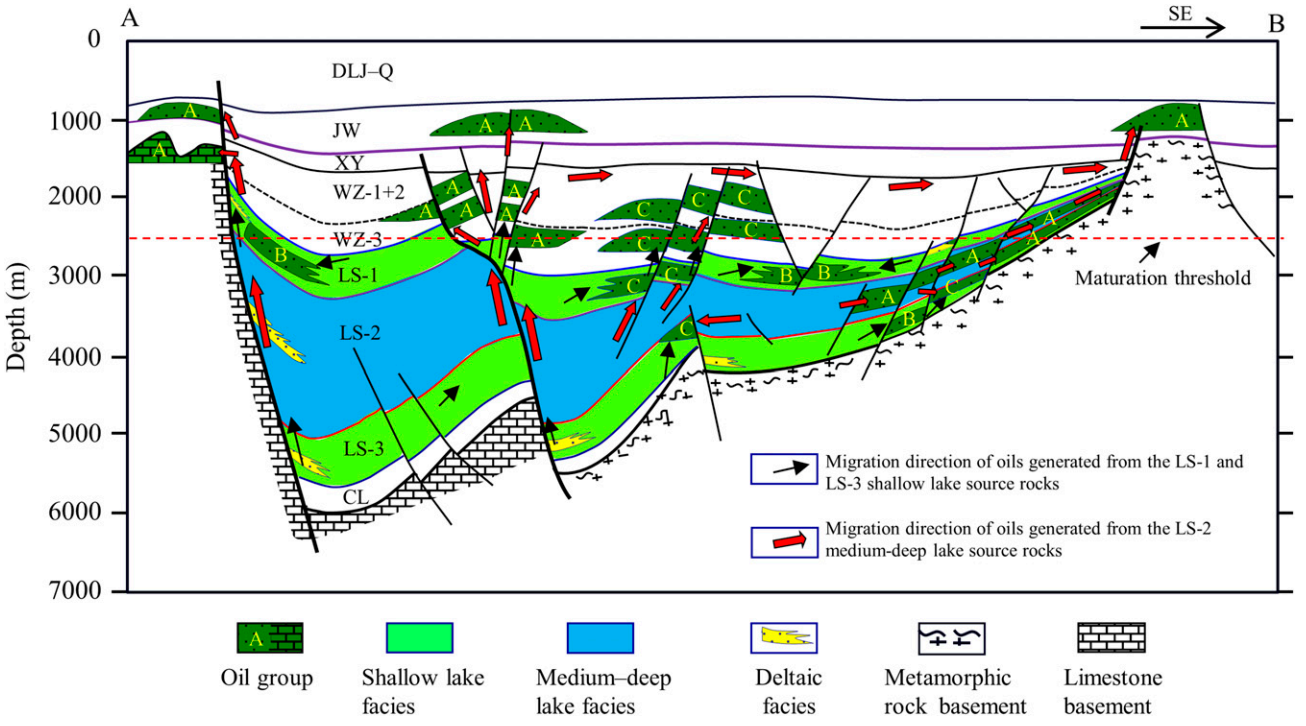

Figure 19. A conceptual model showing oil migration and distribution patterns in the Weixinan and Wushi subbasins. Three migration and distribution patterns for group A oils (indicated by A) are identified: (1) the oils generated from the middle member of the Liushagang Formation (LS-2) medium–deep lake source rocks migrated locally into adjacent reservoirs within the LS-2 member, (2) the oils migrated upward along fractures and faults into the shallow traps of Weizhou Formation, and (3) the oils migrated laterally and/or vertically into the traps on the uplifts and slopes. The latter two migration patterns would certainly move some oils generated from the lower member of the Liushagang Formation (LS-3) and upper member of the Liushagang Formation (LS-1) shallow lake source rocks to the shallow traps, but the oils derived from the LS-2 medium–deep lake source rocks are so huge in volume that the oils from the LS-3 and LS-1 source rocks are geochemically masked, leaving the reservoired oils to display mainly the characteristics of medium–deep lake source rocks. The restricted distribution of group B oils (indicated by B) (only discovered within the LS-3 and LS-1 members) suggests a local migration from the nearby source kitchen. The two migration patterns of group C oils (indicated by C) (mixed oils) include (1) vertical migration to shallow reservoirs along faults that cut or are connected with both medium–deep and shallow lake source rocks and (2) restricted local migration from the nearby LS-3 and the overlying LS-2 source rock layers. The location of the section is shown in Figure 1B. Formation names: CL = Changliu (62.5–58.5 Ma); DLJ = Dengliujiao Quaternary (DLJ–Q = 10.5–0 Ma); JW = Jiaowei (16.5–10.5 Ma); LS = Liushagang (58.5–32 Ma; LS-3 = 58.5–47.5 Ma, LS-2 = 47.5–39.5 Ma, and LS-1 = 39.5–32 Ma); Q = Quaternary; WZ = Weizhou (32–25 Ma); WZ-1+2 = Upper and Middle Weizhou Formation; WZ-3 = Lower Weizhou Formation; XY = Xiayang (25–16.5 Ma).

1230 m [4035 ft]). This further implies that all the oils are derived from similar source kitchens of medium–deep lake source rocks and have migrated upward and accumulated in shallow reservoirs (Figure 19).

For the oils discovered in the uplifts and slopes of the two subbasins, a third migration model is required. Their isotope and biomarker data (Figures 17, 18, Table 3) indicate that these oils were sourced from the medium–deep lake shales. However, the maturation and burial histories reveal that the source rocks nearby these traps are immature for hydrocarbon generation. These oils, therefore, must have migrated laterally (~5–20 km [~3–12 mi]; Liu, 2004; Wang et al., 2014) from areas where the LS-2 medium–deep lake source rocks are thermally mature. As mentioned above, the LS-2 member is deposited in medium–deep lake environments and contains the thickest and most widespread source rocks in the Weixinan and Wushi subbasins, and a major part of this source rock is within the main stage of present-day oil generation. As illustrated in Figure 19, the shallow strata, such as the Jiaowei, Xiayang, and Weizhou Formations (within the subbasins) as well as the Carboniferous on uplifts, are connected by some boundary faults. These faults, along with the connected sandstone

bodies and minor fractures, provide good upward migration pathways for the oils generated in deep source kitchens (Figure 19) to accumulate in the shallow reservoirs of WZ123, WZ128, and WS15 oil fields (Figure 16).

The mixed oils (group C oils) are mainly identified in the shallow Weizhou Formation and LS-1 and LS-3 sandstone traps (Table 3). As illustrated in Figure 19, most of these oils might have migrated upward along the fractures and faults that cut through both the medium–deep lake source rocks in LS-2 member and the shallow lake source rocks in LS-1 or LS-3 members and accumulated in the Weizhou Formation and LS-1 reservoirs, forming the WZ68 and WZ69 oil fields (Figures 18, 19). In addition, some mixed oils are also locally present in the top part of the LS-3 member, and those oils are most likely derived from both the nearby source rock layers of the LS-3 member and the overlying LS-2 source rock layers (Figure 19); the oil field related to this migration pattern includes the WZ122 and WZ118 oil fields (Figure 16).

In summary, these oil migration patterns not only explain the present occurrences of various groups of oils on the uplifts and slopes but also indicate that the shallow traps, especially those close to the faults that cut through or are connected with the source rocks, would provide other favorable places for oil accumulation.

CONCLUSIONS

1. The Eocene lacustrine LS in the BBW Basin contains two different organic facies: the medium–deep lake algal-dominated organic facies in the LS-2 member and the shallow lake mixed algal–terrigenous organic facies in the LS-1 and LS-3 members. The medium–deep lake mudstones in the LS-2 have high TOC values ranging from 2.84 to 14.77 wt. %, and the organic matter in them is dominated by type I and II_1 kerogens with predominantly amorphous macerals, indicating good–excellent oil-prone source potential. The shallow lake mudstones in the LS-1 and LS-3 members display TOC values ranging from 1.5 to 3.7 wt. % and contain mainly type II_1–II_2 kerogens with mixed macerals of AOM, internites, and vitrinites, indicating they are fair to good oil-prone source rocks.
2. The medium–deep lake organic facies is characterized by a high abundance of C_{30} 4-methylsteranes as well as heavy carbon isotopic values, reflecting a dominant algal contribution to the organic matter. Based on the data of biomarkers, stable carbon isotopic values, organic macerals, and V/(V + Ni) ratios, this type of organic facies is interpreted to have been deposited in an anoxic medium–deep lake in a subtropical setting, with diminished water circulation and a permanent water stratification. The high TOC content is attributed to both high plankton productivity and an anoxic water column. In contrast, the mudstones in the shallow lake organic facies display a relatively low abundance of C_{30} 4-methylsteranes and lighter carbon isotopic values. This type of facies was deposited mainly in a dysoxic shallow lake environment with increased input of terrigenous organic matter.
3. Three oil groups (A, B, and C) are identified by their molecular characteristics and stable carbon isotopes. Most of the oils discovered in the Weixinan and Wushi subbasins belong to group A oils and are derived from the Eocene LS-2 medium–deep lake source rocks. Group B oils discovered in the LS-1 and LS-3 reservoirs are sourced from the LS-1 and LS-3 shallow lake source rocks, respectively. Group C oils display intermediate molecular and isotopic compositions between group A and C oils, indicating a mixed source from both shallow lake and medium–deep lake source rocks. The oil–source correlation results illustrate a strong control of organic facies on the oil distribution in the basin.

REFRENCES CITED

Alexander, R., R. A. Noble, and R. J. Kaqi, 1987, Fossil resin biomarkers and their application in oil to source rock correlation, Gippsland basin, Australia: Australian Petroleum Exploration Association Journal, v. 27, p. 63–72.

Bohacs, K. M., A. R. Carroll, J. E. Neal, and P. J. Mankiewicz, 2000, Lake-basin type, source potential, and hydrocarbon character: An integrated sequence-stratigraphic -geochemical framework, *in* E. H. Gierlowski-Kordesch and K. R. Kelts, eds., Lake basins through space and time: AAPG Studies in Geology 46, p. 3–34.

Brassell, S. C., G. Sheng, J. Fu, and G. Eglinton, 1988, Biological markers in lacustrine Chinese oil shales, *in* A. J. Fleet, K. Kelts, and M. R. Talbot, eds., Lacustrine petroleum source rocks: Geological Society, London, Special Publication 1998: v. 40, p. 299–308, doi:10.1144/GSL.SP.1988.040.01.24.

Carroll, A. R., and K. M. Bohacs, 2001, Lake-type controls on petroleum source rocks potential in nonmarine basins: AAPG Bulletin, v. 85, no. 6, p. 1033–1053.

Clayton, C. J., 1991, Effect of maturity on carbon isotope ratios of oils and condensates: Organic Geochemistry, v. 17, no. 6, p. 887–899, doi:10.1016/0146-6380(91)90030-N.

Curiale, J. A., and M. R. Gibling, 1994, Productivity control on oil shale formation—Mae Sot Basin, Thailand: Organic Geochemistry, v. 21, p. 67–89, doi:10.1016/0146-6380(94)90088-4.

Didyk, B. M, B. R. T. Simoneit, S. C. Brassell, and G. Eglinton, 1978, Organic geochemical indicators of paleoenvironmental conditions of sedimentation: Nature, v. 272, no. 5650, p. 216–222, doi:10.1038/272216a0.

Espitalié, J., M. Madec, B. Tissot, J. J. Mennig, and P. Leplat, 1977, Source rock characterization method for petroleum exploration: 9th Annual Offshore Technology Conference, Houston, Texas, May 2–5, 1977, OTC-2935-MS, 6 p., doi:10.4043/2935-MS.

Freeman, K. H., S. G. Wakeham, and J. M. Hayes, 1994, Predictive isotopic biogeochemistry: Hydrocarbons from two anoxic marine basins: Organic Geochemistry, v. 21, p. 629–644, doi:10.1016/0146-6380(94)90009-4.

Fry, B., and E. B. Sherr, 1984, $\delta^{13}C$ measurements as indicators of carbon flow in marine and freshwater ecosystems: Contributions in Marine Science, v. 27, p. 13–47.

Gong, Z. S., and S. Li, 1997, Continental margin basin analysis and hydrocarbon accumulation of the Northern South China Sea (in Chinese with English abstract): Beijing, China, Science Press, 458 p.

Goodwin, N. S., A. L. Mann, and R. C. Patience, 1988, Structure and significance of C_{30} 4-methyl steranes in lacustrine shales and oils: Organic Geochemistry, v. 12, p. 495–506, doi:10.1016/0146-6380(88)90159-3.

Gransch, J. A., and J. Posthuma, 1974, The origin of sulphur in crudes, *in* B. Tissot and F. Beinner, eds., Advances in organic geochemistry 1973: Paris, Editions Technip, p. 727–739.

Harris, N. B., K. H. Freeman, R. D. Pancost, T. S. White, and G. D. Mitchell, 2004, Lacustrine source rocks in the Lower Cretaceous synrift section, Congo Basin, West Africa: AAPG Bulletin, v. 88, no. 8, p. 1163–1184, doi:10.1306/02260403069.

Hatch, J. R., and J. S. Leventhal, 1992, Relationship between inferred redox potential of the depositional environment and geochemistry of the Upper Pennsylvanian (Missourian) Stark Shale Member of the Dennis Limestone, Wabaunsee County, Kansas, USA: Chemical Geology, v. 99, p. 65–82, doi:10.1016/0009-2541(92)90031-Y.

Hollander, D. J., and J. A. McKenzie, 1991, CO_2 control on carbon isotope fractionation during aqueous photosynthesis: A paleo-P_{CO2} barometer: Geology, v. 19, p. 929–932.

Huang, B. J., H. Tian, R. W. T. Wilkins, X. M. Xiao, and L. Li, 2013, Geochemical characteristics, palaeoenvironment and formation model of Eocene organic-rich shales in the Beibuwan Basin, South China Sea: Marine and Petroleum Geology, v. 48, p. 77–89, doi:10.1016/j.marpetgeo.2013.07.012.

Huang, B. J., X. M. Xiao, and M. Q. Zhang, 2003, Geochemistry, grouping and origins of crude oils in the Western Pearl River Mouth Basin, offshore South China Sea: Organic Geochemistry, v. 34, p. 993–1008, doi:10.1016/S0146-6380(03)00035-4.

Huang, D., 1993, Distribution of carbon in organic matters of continental source rocks (in Chinese with English abstract): China Offshore Oil & Gas, v. 7, p. 1–5.

Ji, L. M., F. Meng, K. Yan, and Z. Song, 2011, The dinoflagellate cyst *Subtilisphaera* from the Eocene of the Qaidam Basin, northwest China, and its implications for hydrocarbon exploration: Review of Palaeobotany and Palynology, v. 167, p. 40–50, doi:10.1016/j.revpalbo.2011.07.005.

Katz, B. J., 1995a, A survey of rift basin source rocks, *in* J. J. Lambiase, ed., Hydrocarbon habitat of rift basins: Geological Society, London, Special Publications 1995, v. 80, 213–240, doi:10.1144/GSL.SP.1995.080.01.11.

Katz, B. J., 1995b, Factors controlling the development of lacustrine petroleum source rocks—An update, *in* A. Y. Huc, ed., Paleogeography, paleoclimate, and source rocks: AAPG Studies in Geology 40, p. 61–79.

Lafargue, F., F. Marquis, and D. Pillot, 1998, Rock-Eval 6 applications in hydrocarbon exploration, production, and soil contamination studies: Oil & Gas Science and Technology—Revue d'IFP Energies Nouvelles, v. 53, p. 421–437.

Liu, M. Q., 2004, The assumed gas accumulation systems in Beibuwan basin (in Chinese): China Offshore Oil & Gas, v. 16, p. 93–97.

Li, M. X., 1994, Paleoclimate, and paleoenvironment in the petroliferous region of the north continental shelf region of South China Sea (in Chinese), *in* Z. X. Zhang, L. Zen, and M. X. Li, eds., Tertiary in Petroliferous region of China (VIII): Beijing, China, Petroleum Industry Press, p. 80–89.

Michael, R. T., and D. A. Livingstone, 1989, Hydrogen index index and carbon isotopes of lacustrine organic matter as lake level indicators: Palaeogeography, Palaeoclimatology, Palaeoecology, v. 70, p. 121–137, doi:10.1016/0031-0182(89)90084-9.

Murray, A. P., I. B. Sosrowindjojo, R. Alexander, R. I. Kagi, C. M. Norgate, and R. E. Summons, 1997, Oleananes in oils and sediments: Evidence of marine influence during early diagenesis?: Geochimica et Cosmochimica Acta, v. 61, p. 1261–1276.

Peters, K. E., C. C. Walters, and J. M. Moldowan, 2005, The biomarker guide, 2nd ed., Cambridge, United Kingdom, Cambridge University Press, 1155 p.

Robison, C. R., L. W. Elrod, and K. K. Bissada, 1998, Petroleum generation, migration, and entrapment in the Zhu 1 depression, Pearl River Mouth basin, South China Sea: International Journal of Coal Geology, v. 37, p. 155–178, doi:10.1016/S0166-5162(98)00023-8.

Rodriguez, N. D., and R. P. Philp, 2015, Source rock facies distribution predicted from oil geochemistry in the Central Sumatra Basin, Indonesia: AAPG Bulletin, v. 99, no. 11, p. 2005–2022, doi:10.1306/06191514050.

Ru, K., and J. D. Pigott, 1986, Episodic rifting and subsidence in the South China Sea: AAPG Bulletin, v. 70, no. 9, p. 1136–1155.

Rullkötter, J., T. M. Peakman, and H. L. ten Haven, 1994, Early diagenesis of terrigenous triterpenoids and its implications for petroleum geochemistry: Organic Geochemistry, v. 21, p. 215–233, doi:10.1016/0146-6380(94)90186-4.

Schouten, S., H. M. E. van Kaam-Peters, W. I. C. Rijpstra, M. Schoell, and J. S. Sinninghe Damsté, 2000, Effects of an oceanic anoxic event on the stable carbon isotopic composition of early Toarcian carbon: American Journal of Science, v. 300, p. 1–22, doi:10.2475/ajs.300.1.1.

Seifert, W. K., and J. M. Moldowan, 1978, Applications of steranes, terpanes and monoaromatics to the maturation, migration and source of crude oils: Geochimica et Cosmochimica Acta, v. 42, p. 77–95, doi:10.1016/0016-7037(78)90219-3.

Seifert, W. K., and J. M. Moldowan, 1986, Use of biological markers in petroleum exploration, *in* R. B. Johns, ed.: Amsterdam, Elsevier, Methods in geochemistry and geophysics 24, p. 261–290.

Sinninghe Damsté, J. S., F. Kenig, M. L. Koopmans, J. Koster, S. Schouten, J. M. Hayes, and J. W. de Leeuw, 1995, Evidence for gammacerane as an indicator of water column stratification: Geochimica et Cosmochimica Acta, v. 59, p. 1895–1900, doi:10.1016/0016-7037(95)00073-9.

Smith, B. N., and S. Epstein, 1971, Two categories of $\delta^{13}C/\delta^{12}C$ ratios for higher plants: Plant Physiology, v. 47, p. 380–384, doi:10.1104/pp.47.3.380.

Song, G. L., M. H. Xi, P. Zhang, and X. G. Li, 2012, Hydrocarbon accumulation characteristics in the Weixinan Sag, Beibuwan Basin (in Chinese): Geology and Exploration, v. 48, p. 415–420.

Sun, W., T. L. Fan, Z. G. Zhao, H. Y. Wang, and Z. Q. Gao, 2008, Paleogene sequence stratigraphy and sedimentary system in the Wushi Sag, Beibuwan Basin (in Chinese): Natural Gas Industry, v. 28, p. 29–32.

ten Haven, H. L., J. W. de Leeuw, J. Rullkötter, and J. S. Sinninghe Damsté, 1987, Restricted utility of the pristine/phytane ratio as a paleoenvironmental indicator: Nature, v. 330, p. 641–643, doi:10.1038/330641a0.

Thomas, J. B., J. Marshall, A. L. Mann, R. E. Summons, and J. R. Maxwell, 1993, Dinosteranes (4, 23,24-trimethylsteranes) and other biological markers in dinoglagellate-rich marine sediments of Rhaetian age: Organic Geochemistry, v. 20, p. 91–104, doi:10.1016/0146-6380(93)90084-O.

Tyson, R. V., 1993, Palynofacies analysis, *in* D. G. Jenkins, ed., Applied micropalaeontology: Dordreht, Netherlands, Kluwer Academic, p. 153–191, doi:10.1007/978-94-017-0763-3_5.

Wang, X. M., M. Z. Wang, and X. Q. Zhang, 2005, Palynology assemblages and paleoclimatic character of the Late Eocene to the Early Oligocene in China (in Chinese): Earth Science-Journal of China University of Geosciences, v. 30, p. 309–316.

Wang, Z. F., X. S. Li, J. Gan, and X. B. Yang, 2014, Petroleum geology and exploration potential in the Beibuwan Basin, the South China Sea (in Chinese): Zhanjiang, China, China National Offshore Oil Corporation Ltd. Internal Report, 218 p.

Yang, S. K., 1995, Huxian Lake in Runnan Province of China, *in* X. C. Jin, ed., Environment of lakes in China: Beijing, China, Ocean Press, p. 211–235.

Zhu, W. L., 2009, Palaeolimnology and hydrocarbon source studies of Cenozoic hydrocarbon-bearing offshore basin in China: Beijing, China, Geological Publishing House, 239 p.

Zhu, W. L., and L. J. Mi, 2010, Atlas of oil and gas basins, China Sea (in Chinese): Beijing, China, Petroleum Industry Press, p. 144–158.

Zhu, W. L., and G. X. Wu, 2004, Palaeolimology and hydrocarbon potential in Beibuwan Basin of the South China Sea (in Chinese with English abstract): Oceanologia et Limnologia Sinica, v. 35, p. 8–14.